Epigenetic drugs as a pharmacological approach in Duchenne Muscular Dystrophy

Dottoranda
Valeria Bianconi

Relatore
Chiara Mozzetta

SAPIENZA
UNIVERSITÀ DI ROMA

SAPIENZA
UNIVERSITÀ DI ROMA

Epigenetic drugs as a pharmacological approach in Duchenne Muscular Dystrophy

Facoltà di Facoltà di Scienze SMFN

Dipartimento di Biologia e Biotecnologie "Charles Darwin"
Dottorato in Biologia cellulare e dello Sviluppo

Valeria Bianconi

Matricola 1648934

Relatore

Chiara Mozzetta

A.A. 2020-2021

INDEX

Summary

Duchenne Muscular Dystrophy (DMD) is the most severe form of dystrophy that leads to progressive muscle weakness because of a gradual replacement of functional muscle with fat and fibrotic scars. Pharmacological therapies for DMD should therefore aim to counteract this fibro-adipogenic degeneration and to promote the compensatory regeneration to slow down progression of pathology. Previous works proved pre-clinical efficacy of pan-histone deacetylase inhibitors (HDACi) in the treatment of murine models of DMD, showing the ability of HDACi to counter disease progression and to induce functional and morphological recovery. These studies paved the way for ongoing clinical trials on dystrophic boys but the use of pan-HDACi raises several concerns because of their lack of selectivity and the potential to induce adverse effects over longer period of treatment. Thus, an urgency in the field of epigenetic pharmacology is to develop more selective strategies. Other epigenetic modifiers, such as Histone Lysine Methyltransferases (KMTs) are emerging as particularly relevant in myogenesis. In particular, Histone 3 Lysine 9 (H3K9) KMTs are implicated in the dynamic control of gene expression in myogenic precursors and are highly specific for their targets. Therefore, the development of KMTs specific inhibitors might be a strategy to increase selectivity of epigenetic therapies. We aimed here to test pre-clinical efficacy of newly developed specific inhibitors for class I HDACs (I-HDACi) and H3K9 KMTs (KMTi) in murine models of skeletal muscle regeneration and DMD. We reason that modulation of these epigenetic modifiers could represent a way to promote the expression of muscle-specific genes and to enhance muscle differentiation in cells or tissues whose myogenic capacity is compromised, such as DMD. In agreement with this idea, we show here that the *in vivo* inhibition of H3K9 KMTs and class I HDACs efficiently promotes an overall muscle regeneration in injured wild type mice and mdx mice (the murine model for DMD). These drugs promote an increasement of myofibers' size, and reduction of adipogenic, fibrotic and inflammatory infiltrations. Our data indicate that the pharmacological treatment with these specific epigenetic drugs might become an effective therapeutic approach to counteract the degeneration in DMD. The results of these studies will provide important insights to further develop these drugs and even to conceive future combined therapies targeting both HDACs and KMTs.

Sommario

La distrofia muscolare di Duchenne (DMD) è la forma più grave di distrofia che porta a progressiva debolezza muscolare a causa di una graduale sostituzione del muscolo con tessuto adiposo e fibrotico non funzionale. Le terapie farmacologiche per la DMD dovrebbero quindi mirare a contrastare questa degenerazione fibro-adipogenica, promuovendo nello stesso tempo la rigenerazione compensatoria al fine di rallentare la progressione della patologia. Studi precedenti hanno dimostrato l'efficacia dell'utilizzo di pan-inibitori delle istone deacetilasi (HDACi) nel trattamento di modelli murini di DMD, mostrando la capacità degli HDACi nel contrastare la progressione della malattia e indurre il recupero funzionale e morfologico. Queste evidenze hanno aperto la strada a studi preclinici su ragazzi distrofici, ma l'uso di pan-HDACi solleva diverse controversie a causa della loro mancanza di selettività e della possibilità di avere effetti collaterali per periodi di trattamento più lunghi. Pertanto, lo sviluppo di strategie più selettive sta diventando cruciale nel campo della farmacologia

epigenetica. Altri modificatori epigenetici, come le lisina metiltransferasi (KMT) stanno emergendo come particolarmente rilevanti nella miogenesi, essendo altamente specifici per precise lisine ed essendo implicati nel controllo dell'espressione genica nei precursori miogenici. Lo sviluppo di inibitori specifici delle KMTs potrebbe quindi essere una valida strategia per aumentare la selettività delle terapie epigenetiche. Il nostro studio mira a testare l'efficacia pre-clinica di nuovi inibitori specifici per HDAC di classe I (I-HDACi) e le KMTs della lisina 9 dell'istone H3 (H3K9) (KMTi) in modelli murini di rigenerazione del muscolo scheletrico e di DMD. La nostra ipotesi è che la modulazione di questi modificatori epigenetici possa rappresentare un modo per promuovere l'espressione di geni specifici del muscolo e migliorare il differenziamento muscolare in cellule, o tessuti, la cui capacità miogenica è compromessa, come nella DMD.
I dati ottenuti evidenziano un effetto pro-rigenerativo di questi inibitori *in vivo*. Infatti, l'inibizione delle H3K9 KMT e delle HDAC di classe I promuove la rigenerazione muscolare sia in topi wild type che in topi mdx (modello murino per la DMD). I muscoli trattati mostrano un aumento dell'area delle miofibre, ed allo stesso tempo, una riduzione dell'infiltrato adipogenico e fibrotico, oltre che dell'infiammazione.
I dati ottenuti suggeriscono che il trattamento farmacologico con questi specifici farmaci epigenetici potrebbe diventare un efficace approccio terapeutico per contrastare la degenerazione nella DMD. I nostri risultati potranno quindi fornire importanti indicazioni per sviluppare ulteriormente questi farmaci e potenzialmente concepire future terapie combinate indirizzate sia all'inibizione di specifiche HDACs che KMTs.

Introduction

Duchenne muscular dystrophy (DMD) is a recessive X-linked disease affecting approximately 1/3500 male born that leads to a rapid muscle degeneration, loss of the ability of autonomous deambulation and premature death in adolescence or early adulthood. This pathology is caused by the absence of a functional Dystrophin protein, a crucial structural component of the Dystrophin-Glycoprotein Complex (DGC) implicated in conferring proper stability and integrity to the sarcolemma of muscle fibers. In DMD patients, dystrophin-deficient myofibers possess increased vulnerability to the mechanical stress imposed by muscle contraction, leading to progressive muscle wasting, caused by rupture of dystrophic myofibers that die after repeated contractions. Fibrotic and adipose tissues accumulate in degenerating dystrophic muscles, thus contributing to skeletal muscle loss of function (Mercuri and Muntoni, 2013).
Currently, there is no definitive cure for DMD and the current treatment is the administration of corticosteroids. Gene repair strategies, such as gene- and/or cell-therapies, represent the most promising curative approach for DMD patients as they aim to correct the genetic defects through a systemic introduction of a functional dystrophin gene into muscles of affected boys (Xu et al., 2016; Guiraud S. and Davies K.E, 2017). On the other hand, also pharmacological approaches whose purpose is to slow down the course of the disease supporting the initial regenerative response, may represent an effective treatment (Mozzetta et al., 2009). Although this kind of approach is not curative, one positive aspect is that pharmacological therapies targeting events downstream the genetic defects are potentially available for all patients without restrictions imposed by the specific DMD mutations. To this end, therapies designed to promote the regenerative capacity of muscle progenitor cells should therefore be beneficial

in improving regeneration of dystrophic muscles and to counteract their fibroadipogenic degeneration.

In physiological skeletal muscle repair, Muscle stem cells (MuSCs), called satellite cells, become activated upon injury and enter the myogenic program to differentiate and to replace damaged muscle fibers. This regenerative response characterizes also the first stages of DMD progression, when MuSCs-mediated regeneration is also supported by Fibro-adipogenic progenitors (FAPs), a muscle resident mesenchymal population, that release paracrine factors to create a favorable environment that supports the formation of new myofibers (Heredia et al., 2013; Joe et al., 2010; Mozzetta et al., 2013). However, as disease progresses muscle mass is replaced with fibrotic and fat tissues and recent studies identified FAPs as the source of fibrotic and fatty infiltrates that accumulate in degenerating dystrophic muscles (Kopinke et al., 2017; Uezumi et al., 2011).

Stem cells differentiation is dynamically controlled by chromatin modifying enzymes that epigenetically regulate the spatio-temporal expression of defined transcriptional programs. These classes of enzymes are now druggable and represent a rich source of potential therapeutic pharmacological targets (Arrowsmith et al., 2012). Among these chromatin modifiers, in the context of myogenesis, HDACs and H3K9 KMTs are attractive candidates as they contribute to epigenetic repression of muscle-specific genes in myogenic precursors and their inhibition has been associated with enhanced myogenesis (Minetti et al., 2006; Ling et al., 2012a; Choi et al., 2014), suggesting that their use *in vivo* should improve myogenic capacity of diseased muscles.

In the context of muscular dystrophy, pivotal studies demonstrated the therapeutic potential of epigenetic drugs such as HDACs inhibitors (HDACi) (Colussi et al., 2008; Consalvi et al., 2013; Minetti et al., 2006; Mozzetta et al., 2013). The rationale behind their use derived from experimental evidence demonstrating that HDACs pharmacological inhibition promote muscle differentiation *in vitro* and *in vivo* (Iezzi et al., 2004). These studies inspired the exploration of preclinical efficacy of HDACi in murine models of muscular dystrophies, which led to demonstrate their beneficial effect in the functional and morphological recovery of dystrophic muscles (Colussi et al., 2008; Consalvi et al., 2013; Minetti et al., 2006). In particular, HDACi countered disease progression by promoting an increased cross-sectional area (CSA) of myofibers, the restoration of muscle force, a decreased inflammatory infiltrate and the prevention of fibrotic scars accumulation, thus hampering muscle loss and the functional decline that are typically observed in dystrophic mice (Minetti et al., 2006; Colussi et al., 2008). In particular one of these compounds (Givinostat) is now in clinical development on dystrophic boys and already showed promising results in blocking DMD progression (Bettica et al.2016). These findings provided proof of concept of the efficacy of an epigenetic therapy for a genetic disease like DMD (Consalvi et al. 2014). However, pan-HDACi lack selectivity for specific HDACs and their precise mechanism of action is still debated (Delcuve et al.2012). The observation that inhibition of class I HDACs is sufficient to exert most of the beneficial effects triggered by pan-HDACi (Colussi et al., 2008), suggests that improving selectivity of epigenetic therapy does not compromise efficacy but also could increase its effect.

In this scenario, more selective epigenetic targets are represented by the highly specific KMTs (Mozzetta et al.2015), whose inhibition will be likely associated to less off-targets effects. In particular, the KMTs specific for histone 3 lysine 9 methylation (H3K9) are mainly responsible for transcriptional repression and chromatin condensation, thus playing an important role in the maintenance of cell-specific gene expression patterns and in response to extracellular stimuli during cell differentiation (Mozzetta et al., 2015). Several H3K9 KMTs have been identified in mammals, among them the mono- and di-methyltransferase G9a and GLP (G9a-

like protein) that act as a hetero-dimer (Shinkai and Tachibana, 2011; Tachibana et al.2005) are emerging as important modulators of gene expression during the differentiation of stem cells, thus imposing themselves as potential pharmacological targets for regenerative medicine.

In the context of muscle differentiation, G9a and GLP have been identified among epigenetic modulators able to maintain the repression of muscle-specific genes both in embryonic precursors and in myoblasts (Ling et al., 2012a; Ling et al., 2012b; Ohno et al., 2013), thus preventing their premature differentiation and acting as spatio-temporal modulators of the myogenic differentiation program. In particular, G9a directly methylates MyoD (Ling et al., 2012a) and MEF2D (Choi et al., 2014) in proliferating myoblasts thus antagonizing their activity required to induce muscle gene transcription (Sartorelli and Puri, 2018). Moreover, G9a directly interacts with Sharp-1 and enhances its ability to transcriptionally repress MyoD target genes (Ling et al., 2012b). Recently, GLP has been also demonstrated to be recruited, and to mediate H3K9 methylation, on muscle specific promoters both in myoblasts and in myogenic embryonic precursors (Ohno et al., 2013). These evidence, together with data accumulated in our laboratory, led us to speculate that modulation of these epigenetic modifiers could represent a way to promote the expression of muscle-specific genes and to enhance muscle differentiation in cells or tissues whose myogenic capacity is compromised, such as DMD. Several selective G9a/GLP inhibitors (KMTi) have been developed (Sweis et al.,2014) (Pappano et al., 2015). but never tested so far on murine models of muscle regeneration and DMD *in vivo*. Therefore, in this work, in collaboration with IRBM (Pomezia, Italy), we tested pre-clinical efficacy of new selective class-I HDACis and newly designed G9a/GLP KMTis on murine models of skeletal muscle regeneration and DMD. Our results provide evidence that these treatments ameliorate the dystrophic phenotype in mdx mice and induce an overall muscle regeneration at the expenses of the fibroadipogenic degeneration, posing a solid basis for the possible future clinical development in DMD patients.

Aim of the work

The aim of this work is to investigate the therapeutic potential of new epigenetic strategies for muscle regeneration and DMD, based on the evaluation of their capacity to enhance myogenesis both *in vitro* and *in vivo*. We assume that the use of more selective compounds will enhance efficacy, safety and tolerability of the epigenetic therapies in DMD.

Despite numerous clinical trials over the last decades have reached significant progress in the treatment of patients with DMD, in terms of slowdown of disease progression, improvement of the quality of life and lengthening life expectancy (Guiraud and Davies, 2017), the cure for DMD is still a challenge.

Previous works proved clinical and pre-clinical efficacy of pan-histone deacetylase inhibitors (HDACi) in the treatment of DMD, showing the ability of HDACi to counter disease progression and induce functional and morphological recovery both in murine models and DMD boys. However, HDACi promote regeneration of dystrophic muscles if administered at early stage of DMD progression, while are ineffective if delivered at advanced stages when dystrophic muscles are already degenerated (Mozzetta et al.,2013). HDACi are able to induce hyperacetylation of pro-myogenic loci in the chromatin of FAPs, thus stimulating their participation to myogenesis at early stages of DMD, when compensatory regeneration is still ongoing (Saccone et al., 2014). By contrast, in degenerated dystrophic muscles FAPs' pro-myogenic loci are resistant to HDACi-induced acetylation and expression, and this correlates with the resistance to HDACi-mediated beneficial effects (Mozzetta et al., 2013; Saccone et al., 2014). These results led us to hypothesize that in degenerating muscles aberrant accumulation of epigenetic silencing factors might constraint FAPs chromatin plasticity preventing remodeling of pro-regenerative loci. Among the different silencing epigenetic modifications, H3K9 methylation is the best characterized and constantly associated with stable epigenetic repression. This prompted our interest in investigating the impact of H3K9 KMTs modulation in DMD murine models, exploring pre-clinical efficacy of H3K9 KMTs inhibitors as a pro-regenerative approach.

Among the variety of H3K9 KMTs, G9a and GLP are excellent candidates as pharmacological targets, as it has been possible to develop very specific and selective inhibitors. Thus, in this work we first characterized the potential of known and new developed G9a/GLP inhibitors to enhance myogenesis on *in vitro* cellular models. Then, we tested their capacity to promote muscle regeneration *in vivo*. Finally, we assessed their potential to prevent fibro-adipogenic degeneration and to hamper DMD progression in dystrophic mice.

In addition, since previous works demonstrated that inhibition of HDACis of class I is sufficient to obtain recovery of DMD in murine model of the disease, with the aim to prove pre-clinical efficacy of more selective epigenetic drugs, we have also tested compounds selective for class I HDACs.

Results

G9a/GLP pharmacological inhibition enhances muscle differentiation in vitro

Since G9a/GLP specific inhibitors were never tested on skeletal muscle cellular models, we first investigated if G9a/GLP inhibition affected skeletal muscle differentiation *in vitro*. To this end, we treated the myoblasts C2C12 cells line with a known G9a/GLP selective competitive inhibitor, A-366 (Pappano et al., 2015), and with a newly developed compound (M-108), designed by our collaborators (IRBM). Cells were treated for 48 hours in growing conditions, and then induced to differentiate in the absence of the inhibitors (fig.1A, left panel). The capacity to form Myosin Heavy Chain (MyHC) positive myotubes was then assessed by Immunofluorescence (IF) for MyHC and quantified by the evaluation of myotubes' diameter. As shown in Fig1A (middle and right panels), C2C12 treated with both A-366 and M-108 displayed the capacity to form bigger myotubes, as compared to control cells treated with DMSO, which indicated an increased differentiation potential.

To understand if G9a/GLP inhibition could also influence the fate of the principal populations involved in skeletal muscle regeneration and degeneration of dystrophic muscles, that is MuSCs and FAPs respectively, we isolated them by Fluorescence Activated Cell Sorting (FACS) from mdx mice (C57BL/10ScSn-*Dmd*^{mdx}/J; 8 weeks old) (Fig. 1B). We then assessed their differentiation capacities upon A-366 and M-108 treatment *ex-vivo*. MuSCs treated in growth medium (GM) for 48 hours with the inhibitors, and then shifted in differentiation medium, formed larger myotubes upon the delivery of M-108, as compared to control-treated (DMSO) MuSCs (fig.1C).

FAPs have been shown to massively differentiate into Perilipin-positive adipocytes when cultured in adipogenic-differentiation medium (Joe et al., 2010; Uezumi et al., 2010). To test if G9a/GLP inhibition might have an impact on FAPs differentiation capacity, we treated mdx FAPs with both A-366 and M108 in GM for 48 hours, and we then shifted them in adipogenic differentiation medium in the absence of the treatment (Fig.1D). IF for perilipin and MyHC revealed that both compounds impaired FAPs adipogenic differentiation, as quantified by the decreased number of Perilipin+ adipocytes (Fig.1D, right panel). Strikingly, either A366 and M108 promoted the formation of MyHC+ myotubes, further supporting a role for G9a/GLP in repressing the myogenic program in FAPs, in agreement with our previous data (Biferali, Bianconi et al., *under revision on Science Advances*).

Taken together, these results indicate that G9a/GLP inhibition exert pro-myogenic effects, and prompted us to test A-366 and M-108 *in vivo* in a mouse model of skeletal muscle regeneration.

Figure 1

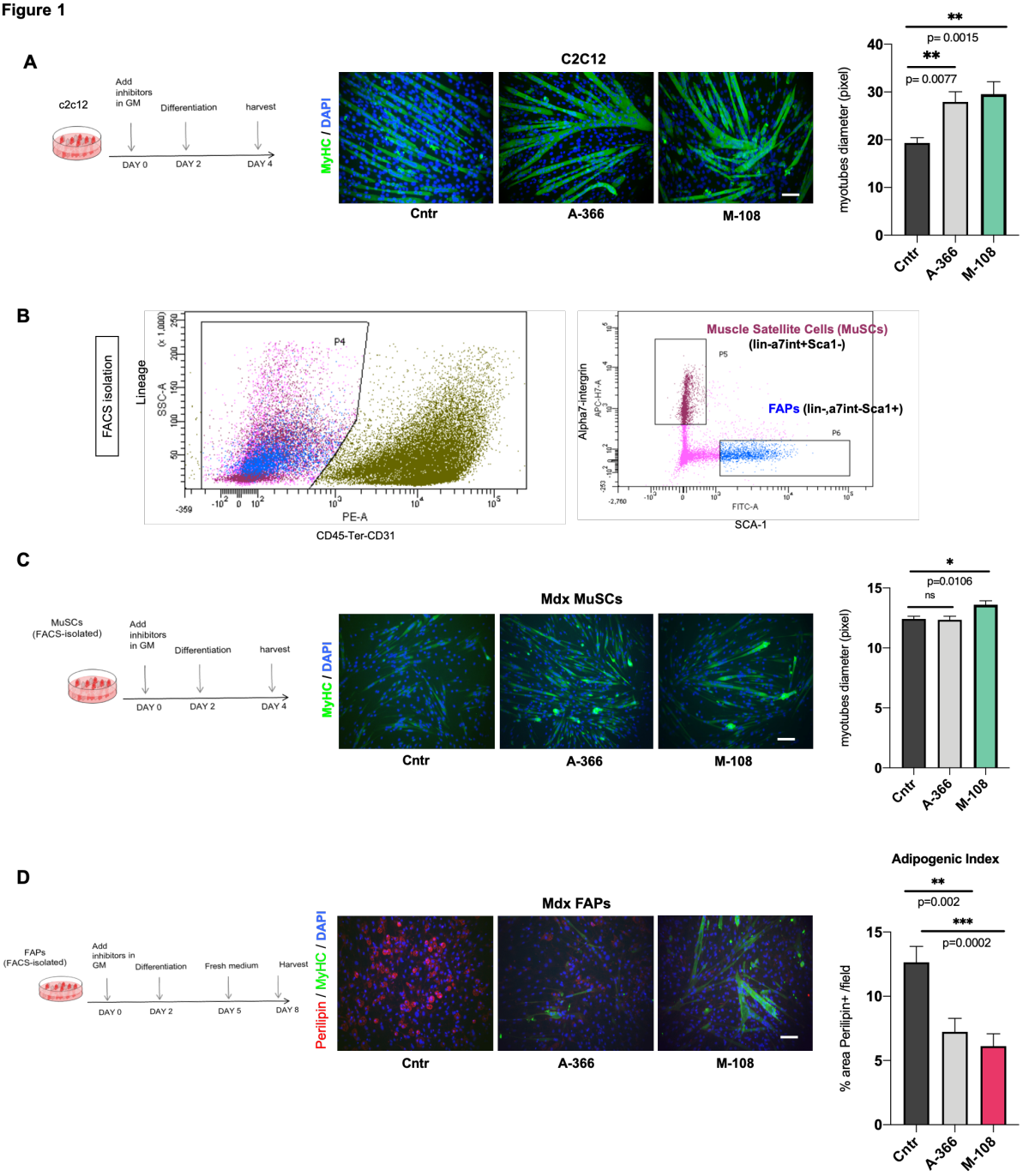

Figure 1: **G9a/GLP pharmacological inhibition enhances muscle differentiation *in vitro* and unmasks FAPs myogenic potential. A)** *Left:* experimental design of the treatment of C2C12 with A366 (1nM) and M-108 (50nM). Cells were treated for 48h in growth medium (GM) and then were induced to differentiate in the absence of the inhibitors. *Middle:* representative images of immunofluorescence (IF) for MyHC (green) and Dapi (blue) of C2C12 cultured as indicated on the left panel. *Right*: quantification of the diameter of myotubes, expressed in pixel. Data are represented as average ± SEM of n=3 independent experiments. **B)** Schematic representation of FACS sorting to isolate MuSCs and FAPs from C57/BL6J or C57BL/10ScSn-Dmdmdx/J mice. Satellite cells (MuSCs) were isolated as Ter119-/CD45-/CD31-/α7Integrin+/Sca1- cells; FAPs as Ter119-/CD45-/CD31-/α7Integrin-/Sca1+ cells.

C) *Left:* experimental design of MuSCs derived from Mdx mice treated with A366 (1nM) and M-108 (50nM). Freshly sorted cells were seeded in GM and then treated for 48h with the inhibitors before inducing differentiation in the absence of the compounds. *Middle*: representative images of the IF for MyHC (green) and Dapi (blue) of MuSCs cultured as indicated on the left panel. *Right*: quantification of the diameter of myotubes, expressed in pixel. Data are represented as average ± SEM (n=3).

D) *Left:* experimental design of FAPs derived from Mdx mice treated with A366 (1nM) and M-108 (50nM). Freshly sorted cells were seeded in GM and then treated for 48h with the inhibitors before inducing the adipogenic differentiation in the absence of the compounds. *Middle*: representative images of the IF for MyHC (green), Perilipin (red) and Dapi (blue) of FAPs cultured as

indicated on the left panel. Right: histogram shows the evaluation of the percentage of perilipin positive area (pixel^2/ field), calculated with ImageJ software. Data are represented as average ± SEM. (n=3). Statistics by One-Way anova.

G9a/GLP inhibition *in vivo* efficiently down-regulates H3K9me2 in skeletal muscles

To provide *in vivo* evidence that G9a/GLP might represent potential pharmacological targets in skeletal muscle regeneration, we evaluated the impact of their inhibition on a murine model of skeletal muscle regeneration on wild type (C57/BL6J) mice. To this end, we performed short term treatments (5 days) using 2 different doses (0.2mg/kg and 2mg/kg) of A-366 (fig.2A) and compared them to mice treated with vehicle solution as controls. To model skeletal muscle regeneration, mice were subjected to intramuscular injection of cardiotoxin (CTX) (10uM) in all the hindlimb muscles (*tibialis anterior, quadriceps* and *grastrocnemius*) (Fig.2A). Because of the lack of evidence in the literature of the use of these inhibitors *in vivo*, we wanted first to understand if they efficiently modulated H3K9 methylation levels in skeletal muscles. Immunofluorescence (IF) for H3K9me2 on injured tibialis anterior cryo-sections showed the decrease in H3K9me2 global levels in A-366-treated muscles, with both doses, as compared to control muscles (fig.2B). This was also confirmed by western blot (WB) analysis on histones extracted from whole muscles (diaphragm) (Fig.2C) or from FACS-isolated MuSCs and FAPs (fig.2D).

Figure 2

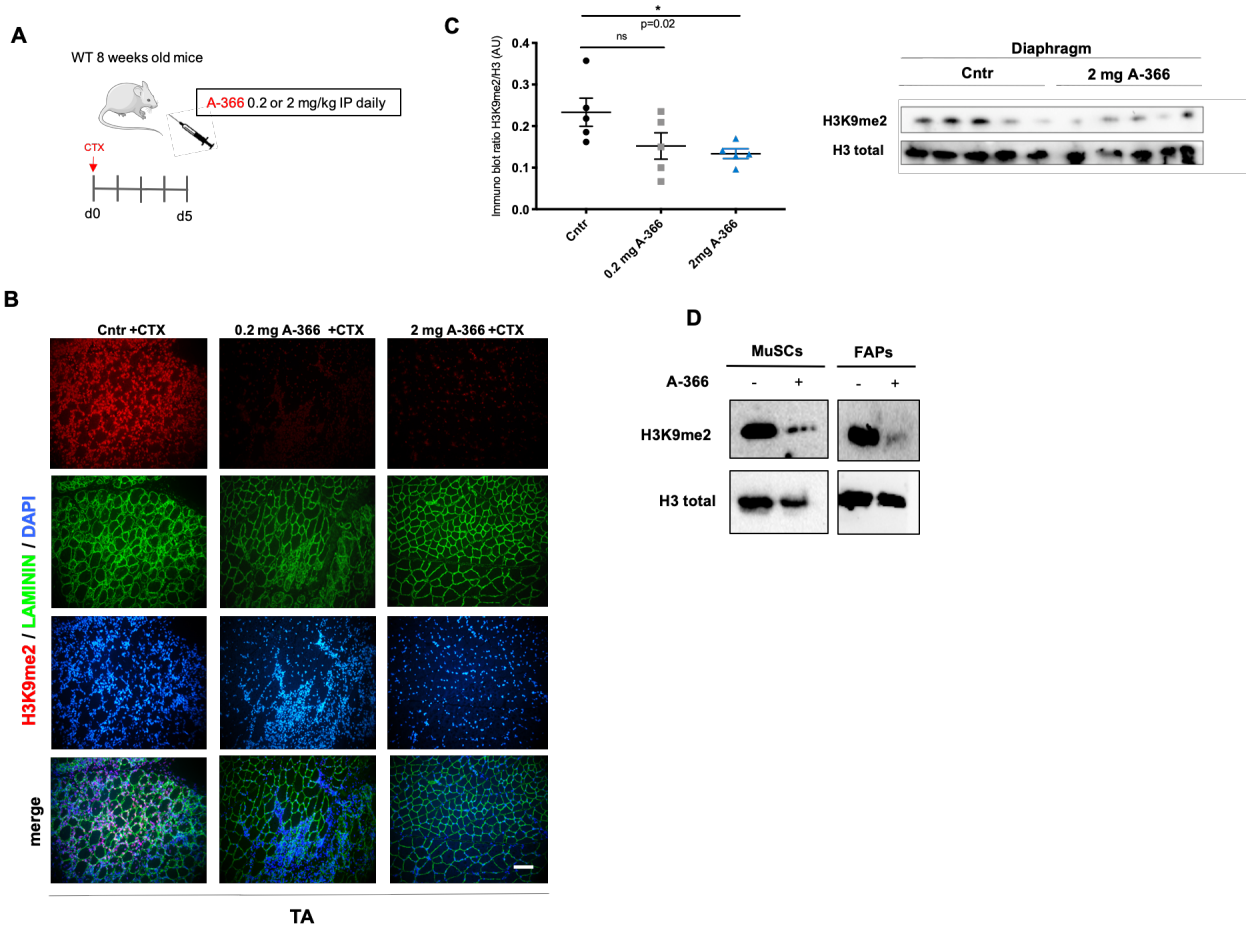

Figure 2: G9a/GLP inhibition *in vivo* efficiently down-regulates H3K9me2 in skeletal muscles. A) Schematic representation of the 5 days long experiment on injured (with cardiotoxin, CTX) wild type mice (C57BL/6) treated in vivo with daily intraperitoneal injection (IP) injection of vehicle (CNTR) or A-366 (0.2 and 2 mg/kg). **B)** Immunofluorescence for H3K9Me2 (red), laminin (green) and nuclei (dapi, blue) on cryosections of tibialis anterior muscles from mice treated as described in (A). **C)** *Right:* dots plot of the quantification of WB analysis on protein extracted from diaphragm (n=5/experimental group) of injured wild type mice treated as in (A), evaluated as the ratio of H3K9me2 levels normalized on total histone H3. Data are represented as average ± SEM. Statistical significance assessed by One way Anova**.** *Left:* representative western blot for H3K9me2 and H3 of diaphragm histones samples from Cntr and A366 2mg-treated mice as described in (A). **D)** Representative Western blot of Cntr and A366 2mg-treated mice samples of histones extracted from FAPs and MuSCs isolated by FACS from muscles treated as described in (A).

G9a/GLP inhibition accelerates myogenic differentiation and promotes muscle regeneration *in vivo*

In light of the results that we obtained *in vitro* (Fig.1), to test the impact of G9a/GLP inhibition *in vivo* on FAPs and MuSCs differentiation capacities, we isolated them from control and A-366 treated mice (Fig.2A) and assessed their differentiation potentials by culturing them *ex vivo* in the absence of any treatment. Strikingly, FAPs isolated from A-366 treated muscles displayed an impaired adipogenic capacity, as demonstrated by the decreased number of Oil-Red O positive adipocytes (Fig.3A). Of note, FAPs isolated from 2mg-A366 muscles, showed also the capacity to form MyHC+ myotubes (Fig.3B), in agreement with what we observed in vitro (Fig.1D).

MuSCs isolated from 2mg-A-366 treated muscles also showed an accelerated differentiation capacity as compared to cells isolated from control muscles (Cntr), since they were able to form MyHC+ myotubes already in growing conditions (Fig.3C). This capacity was likely caused by an augmented proliferation potential, that we assessed by EdU assay (Fig.3C). Accordingly, when induced to differentiate, MuSCs derived from A-366 treated muscles formed also larger myotubes as compared to cells derived from Cntr muscles (Fig.3D). The evidence of an acceleration in muscle differentiation was also paralleled by an overall promotion of muscle regeneration *in vivo*. Evaluation of myofibers cross sectional area (CSA) on Laminin-stained muscle cryosections, and of the number of myofibers expressing the embryonic form of MyHC (eMyHC), a MyhC isoform specifically expressed by newly-formed immature myofibers, showed that G9a/GLP inhibition increased CSA and decreased the percentage of eMyHC+ fibers (Fig.3 E, F, G). The increase of the mean myofibers area accompanied by a reduction in the number of immature myofibers, led us to interpret these results as an accelerated regeneration, which we think is due by the capacity to promote MuSCs differentiation, and in part by FAPs' participation to myogenesis. Moreover, the evidence that G9a/GLP inhibition impairs FAPs adipogenic capacity suggested that such strategy might be used to also block fibro-adipogenic degeneration of dystrophic muscles and prompted our interest in testing these compounds on DMD murine model.

Figure 3

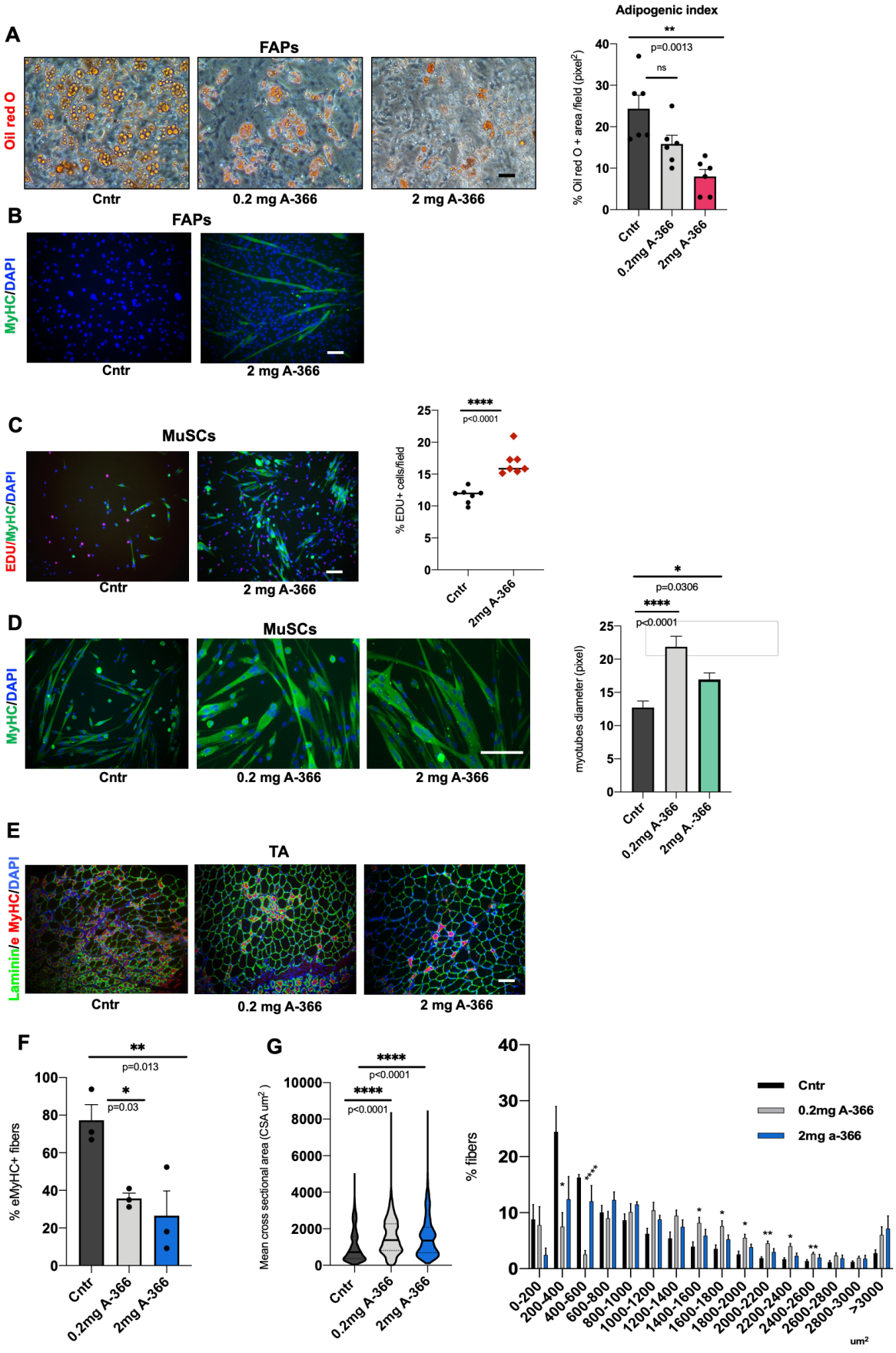
A
FAPs
Oil red O
Cntr
0.2 mg A-366
2 mg A-366
Adipogenic index
**
p=0.0013
ns
% Oil red O + area /field (pixel²)
Cntr
0.2mg A-366
2mg A-366
B
FAPs
MyHC/DAPI
Cntr
2 mg A-366
C
MuSCs
EDU/MyHC/DAPI
Cntr
2 mg A-366
****
p<0.0001
% EDU+ cells/field
Cntr
2mg A-366
D
MuSCs
MyHC/DAPI
Cntr
0.2 mg A-366
2 mg A-366
*
p=0.0306
****
p<0.0001
myotubes diameter (pixel)
Cntr
0.2mg A-366
2mg A-366
E
TA
Laminin/e MyHC/DAPI
Cntr
0.2 mg A-366
2 mg A-366
F
**
p=0.013
*
p=0.03
% eMyHC+ fibers
Cntr
0.2mg A-366
2mg A-366
G
****
p<0.0001
****
p<0.0001
Mean cross sectional area (CSA um²)
Cntr
0.2mg A-366
2mg A-366
% fibers
Cntr
0.2mg A-366
2mg a-366
0-200
200-400
400-600
600-800
800-1000
1000-1200
1400-1600
1600-1800
1800-2000
2000-2200
2200-2400
2400-2600
2600-2800
2800-3000
>3000
um²

Figure 3: G9a/GLP inhibition *in vivo* accelerates myogenic differentiation and promotes muscle regeneration. A) Oil Red O (ORO) staining on FAPs isolated from mice treated as described in (Fig, 2A) and cultured in GM for 5 days and then induced to differentiate in adipogenic medium (DM). ImageJ software was used to quantify the percentage of ORO+ area as pixel^2/field, as show in the graph on the right. Mean +/- sem, statistics by One-way Anova, n=6. **B)** IF for MyHC (green) and nuclei (dapi, blue) of FAPs isolate from Cntr and A366 2mg-treated mice (as in Fig2A) and cultured as described in Fig.3A. **C)** IF for EdU (red), MyHC (green) and nuclei (dapi, Blue) on MuSCs isolated by FACS from mice treated as described in Fig.2A and cultured in GM for 5 days. On the right the graph shows the % of EdU+ cells/field. Mean +/- sem, statistics by One-way Anova, n=6. **D)** *Left:* IF for MyHC (green) and nuclei (dapi, blue) of MuSCs isolated by FACS from mice treated as described in Fig.2A and induced to differentiate. *RIght:* quantification of the diameter of myotubes, expressed in pixel. Mean +/- sem, statistics by One-way Anova, n=7. **E)** IF for eMyHC (red), laminin (green) and nuclei (dapi, blue) on cryosections of tibialis anterior muscles from mice treated as described in Fig. 2A. **F)** Quantification of the % of eMyHC+ myofibers of muscles showed in (E). Mean +/- sem, statistics by One-way Anova, n=3. **G)** *Left:* Violin plot showing distribution of single myofibers CSA of muscles shown in (E)*;* statistics by One-way Anova. *Right:* % of myofibers with CSA within the shown ranges. Data are represented as average ± SEM. (N=5). Statistical significance assessed by Two-way Anova.

G9a/GLP inhibition induces morphological recovery of dystrophic muscles

After the preliminary experiments on a skeletal muscle regeneration mouse model, we decided to test the impact of KMTis in the progression of DMD. To this end, we treated 8 weeks old dystrophic mdx mice (Grounds et al., 2008; De Luca et al.,2012), with daily intraperitoneal injection of A-366 and a the newly developed G9a/GLP specific inhibitor M108, for 45 days; a group of mice treated only with vehicle served us as controls (fig.4A). The results obtained from our previous experiment (Fig.3) were useful to also choose the best dose to use on murine model of disease (2mg/kg).

We first analyzed the effective reduction of H3K9 methylation by WB analysis for H3K9me2, which confirmed that both KMTis reduced of about 50% H3K9me2 levels on whole muscles (fig.4B). Morpho-histological analyses were then used to assess the impact on the dystrophic phenotype. Analysis of CSA demonstrated an increased caliber of single myofibers in muscles from KMTi-treated mice, as compared to controls (fig.4C-D and F). This was accompanied by an increased percentage of center-nucleated fibers in muscles treated with both A366 and M-108 (fig.4E). Taken together, these evidence clearly indicate that G9a/GLP inhibitors promote myogenesis also in dystrophic muscles.

In light of these positive results on myofibers' size, we then tested if G9a/GLP inhibition could prevent the deposition of adipose tissue, a typical detrimental effect of DMD progression. To assess this, we stained muscle cryosection for Oil Red O, an histological analysis that highlights adipocytes infiltration (fig.5A, *upper panels*), and performed an immunofluorescence for Perilipin (Fig.5A, lower panels). Quantification of both staining (Fig. 5A, *right*) demonstrated that G9a/GLP inhibitors significantly reduced the adipogenic infiltration in dystrophic muscles.

The fibrotic scars that characterize hindlimb muscles and the diaphragm in DMD are composed by collagen deposit. To assess the extent of fibrotic deposition after the treatment with KMTis, an immunofluorescence for Collagen3A and a staining for collagen I by Sirius red (fig.5B), on Tibialis anterior (TA) revealed that G9a/GLP inhibition decreased also the fibrotic infiltration in dystrophic muscles. The same stainings on diaphragm (Fig.5C) highlight a significant decreased of the collagen 3A depositions.

Moreover, we assessed the extent of infiltration by staining control and KMTis-treated muscles with myeloperoxidase (MPO), which is expressed by monocytes and macrophages during degeneration of muscle tissue. Strikingly, the delivery of both G9a/GLP inhibitors efficiently reduced the content of MPO+ cells (fig.5D), indicating the capacity of KMTis to also reduce the inflammation of DMD muscles.

Finally, to evaluate a potential functional recovery in mdx mice after the delivery of KMT inhibitors, we treated for 45 days another set of young mdx mice only with A-366 and we performed tests, such as hanging wire (Aartsma-Rus et al., 2014) and treadmill (Denti et al., 2006: Minetti et al., 2006), to assess muscle function. Specifically, control and A366-treated mdx were subjected to the hanging wire test, (as in SOP DMD_M.2.1.004 on treat-nmd.org) every 7 days along the 45 days-long treatment. This test is based on the latency of a mouse to fall off a metal wire upon exhaustion, allowing to assess the natural course of the disease or the efficacy of a pharmacologic treatment in muscle strength. Despite this test highlighted a considerable individual variability among the tested animals and did not detect statistically significant differences, the experimental group of A366-treated mice showed a tendency to an increased hanging time, suggesting a trend in improving muscle function (Fig.6A). At the end of the treatment, the mice were subjected to treadmill test (Fig.6B), which allows to quantify the resistance to fatigue by determining the time to exhaustion and the total distance run by the animal (SOP treatNMD, DMD_M.2.1.001 and DMD_M.2.1.003 on treat-nmd.org). However, this test did not highlight statistically significant differences between the experimental groups. By contrast, evaluation of the number of degenerating fibers, by staining for murine IgG, on cryosections of skeletal muscles derived from control and A366-treated mice subjected to treadmill test showed that A366 reduced the number of necrotic (IgG+) fibres (Fig 6C). This evidence led us to conclude that G9a/GLP inhibition might exert a protective effect against necrosis. This was also corroborated by the evaluation of Creatine Kinase (CK) levels that demonstrated a significant decrease of CK levels in the serum of A366-treated mice as compared to control animals (Fig.6D). Overall, our data demonstrate that strategies aimed at inhibiting G9a/GLP exert both morphological recovery and protective effect on dystrophic muscles.

Figure 4

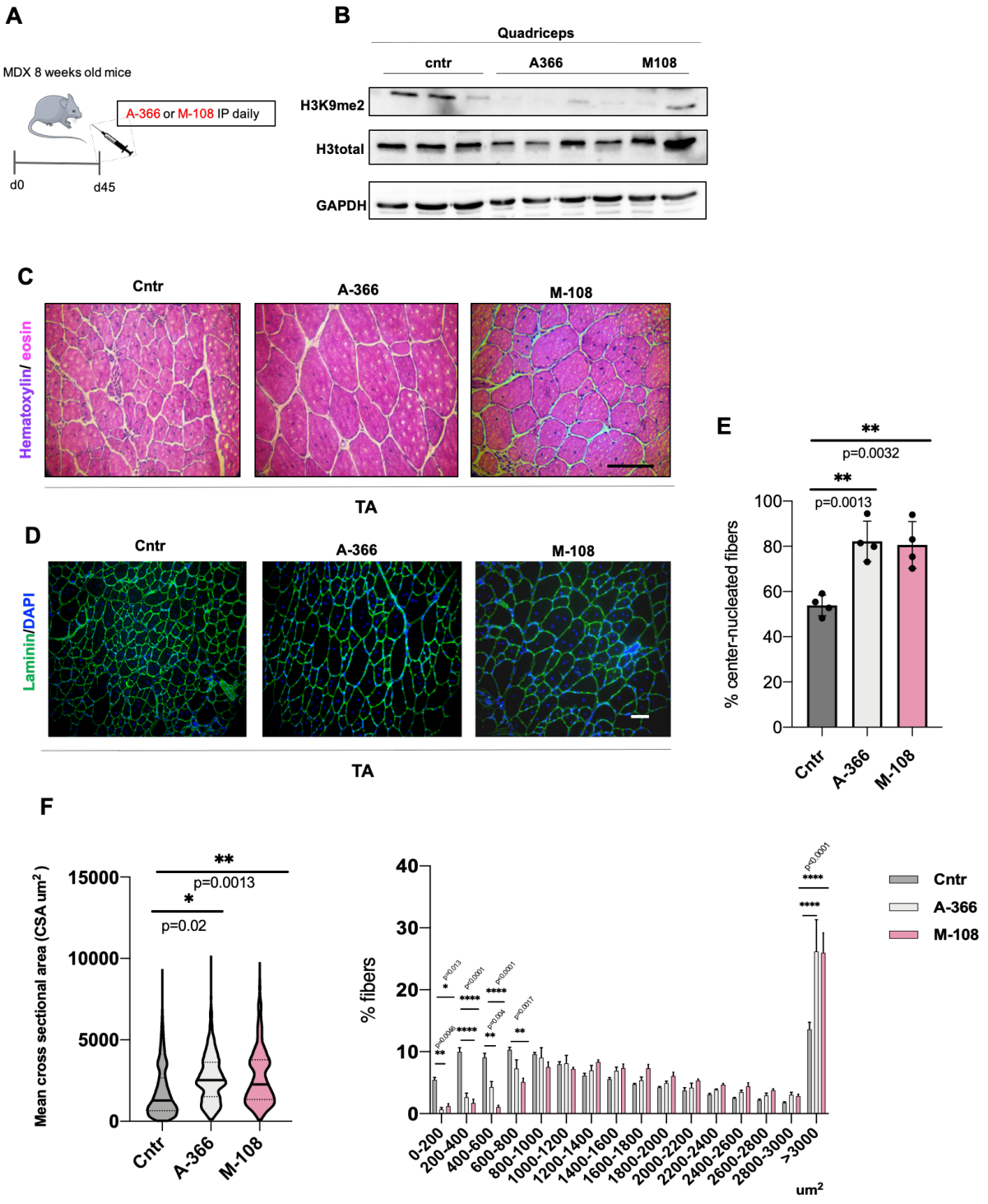

Figure 4: G9a/GLP inhibitors delivery in mdx mice increases myofibers' size. A) representative scheme of the 45 days long experiment on mdx mice treated every day with vehicle (cntr), A-366 or a newly developed G9a/GLP specific inhibitor (M-108). **B)** Representative Western blot for histones extracted from quadriceps isolated from mdx mice treated as described in (A). (N=3). **C)** Staining for Hematoxylin/ Eosin of tibialis anterior from mdx mice treated for 45 days as described in (A). **D)**IF for laminin (green) and nuclei (dapi, blue) on cryosections of tibialis anterior from mdx mice treated as described in (A). **E)** Quantification of center-nucleated fibers of muscles shown in (D). N=4, data are represented as average ± SEM. Statistical significance assessed by One-way anova. **F)** *Left:* Violin plot showing distribution of single myofibers CSA of muscles shown in (D)*;* statistics by One-way Anova. *Right:* % of myofibers with CSA within the shown ranges. Data are represented as average ± SEM. (N=5). Statistical significance assessed by Two-way Anova.

Figure 5

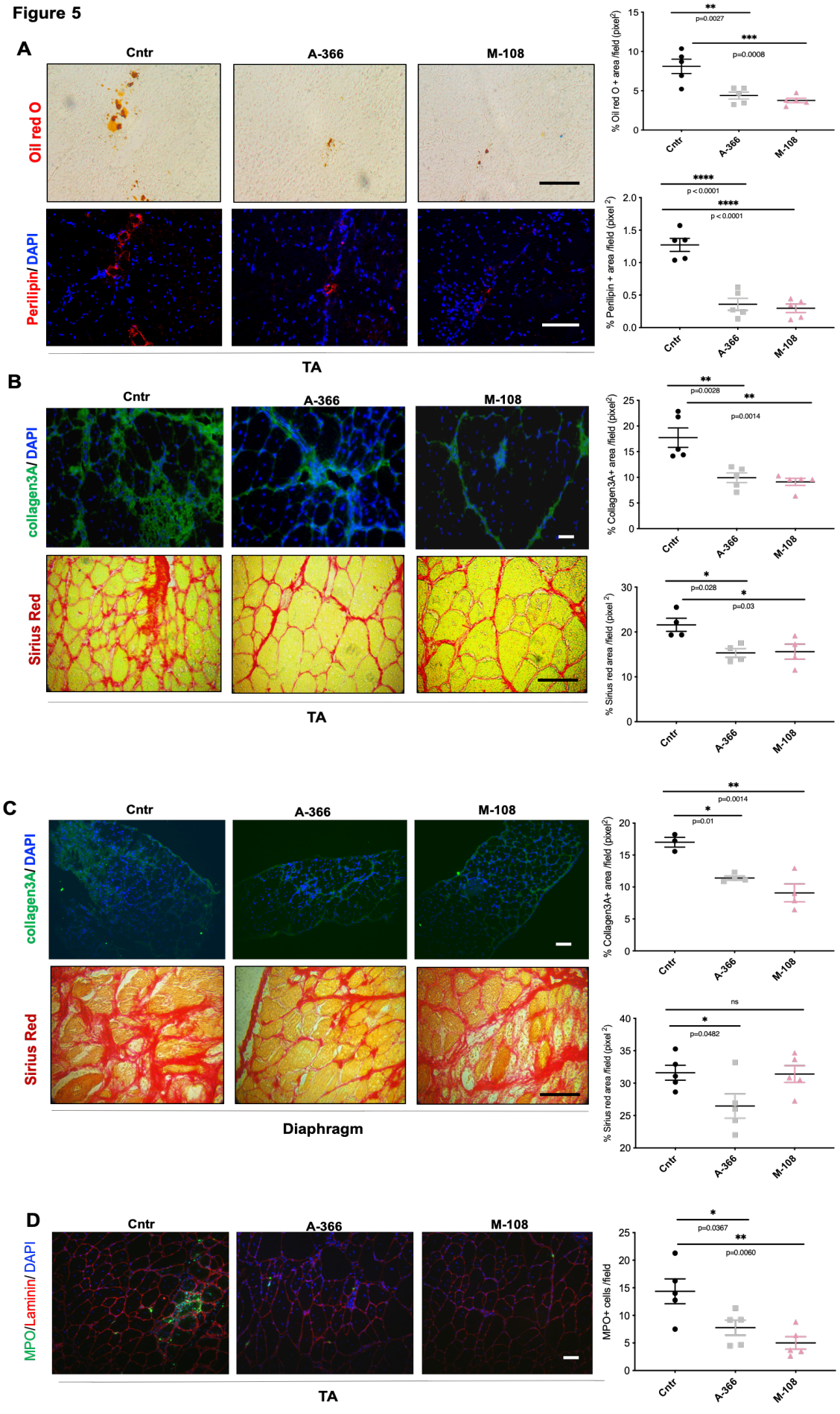
A
Cntr
A-366
M-108
Oil red O
Perilipin/ DAPI
TA
% Oil red O + area /field (pixel²)
p=0.0027
p=0.0008
% Perilipin + area /field (pixel ²)
p < 0.0001
p < 0.0001
B
collagen3A/ DAPI
Sirius Red
TA
% Collagen3A+ area /field (pixel²)
p=0.0028
p=0.0014
% Sirius red area /field (pixel ²)
p=0.028
p=0.03
C
collagen3A/ DAPI
Sirius Red
Diaphragm
% Collagen3A+ area /field (pixel²)
p=0.0014
p=0.01
% Sirius red area /field (pixel ²)
ns
p=0.0482
D
MPO/Laminin/ DAPI
TA
MPO+ cells /field
p=0.0367
p=0.0060

Figure 5: G9a/GLP inhibitors delivery in mdx mice increases myofibers' size and reduce inflammatory, adipogenic and fibrotic infiltrates. A) *Upper panels:* Staining for Oil Red O of muscles treated as in Fig. 4A. *Lower panels:* IF for perilipin (red), and nuclei (dapi, blue), of muscles treated as in Fig. 4A. *Right:* upper graph shows the percentage of the ORO+ area as pixel^2/field. Lower graph shows the percentage of Perilipin+ area as pixel^2/field. Data calculated with ImageJ software and represented as average ± SEM. n=5; statistics by One-way Anova. **B-C)** *Upper panels:* IF staining for Collagen3A (green) and nuclei (dapi, blue) on cryosections of TA (B) and diaphragms (C) muscles from mdx mice treated as in Fig. 4A. *Lower panels:* Sirius Red staining in muscles TA and diaphragms from mdx mice treated as in Fig. 4A. Graphs on the right show quantification of the correspondent stainings. Data calculated with ImageJ software. Data are represented as average ± SEM. n=5; statistics by One-way Anova. **D)** *Left:* IF for Myeloperoxidase (MPO; green), Laminin (red) and nuclei (dapi, blue) on tibialis anterior from mdx mice treated as in Fig. 4A. *Right:* the graph shows quantification of the percentage of MPO positive cells in muscles shown on the left. Data are represented as average ± SEM. n=5; statistics by One-way Anova.

Figure 6

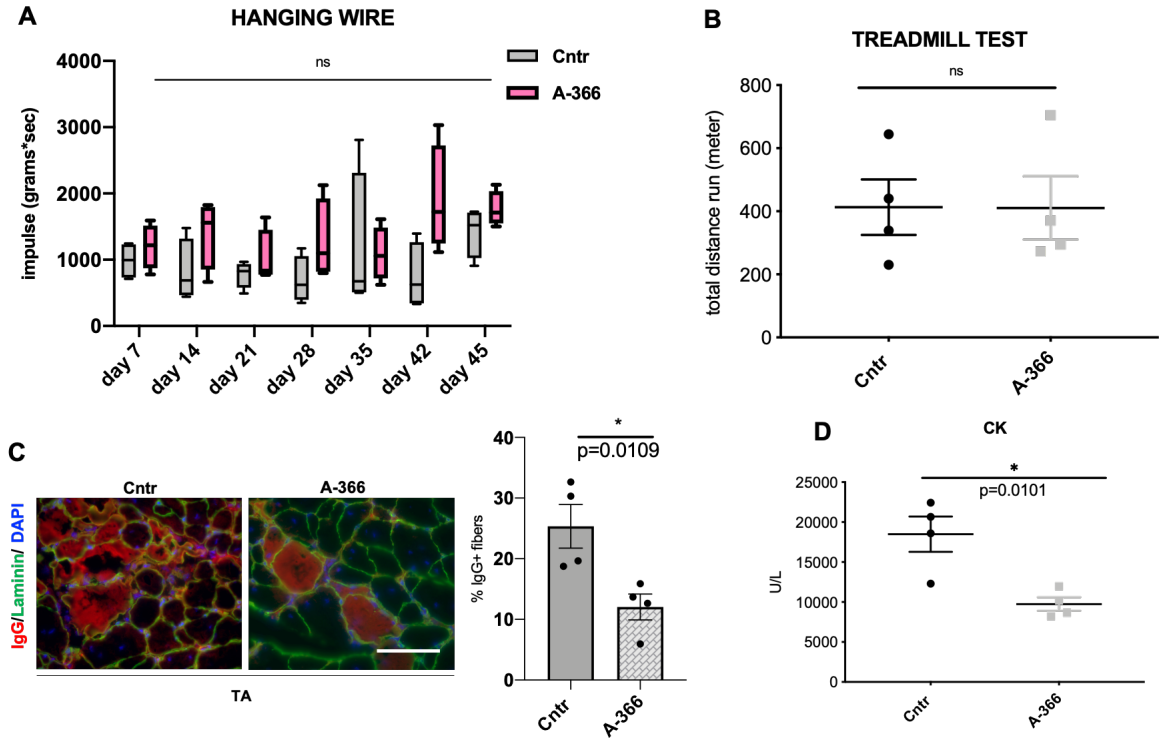

Figure 6: G9a/GLP inhibition protects dystrophic muscles from necrosis. A) Box plot shows quantification of hanging wire test, represented as impulse (seconds x grams), performed every 7 days along a 45d long treatment. Data are represented as average ± SEM and statistically assessed by two way Anova (N=4). **B)** Quantification of Treadmill test perfromed at day 45, representing the total amount of meters run by each mouse. Data are shown as average ± SEM; statistics assessed by t-test (N=4). **C)** Left: representative images of IgG staining (red), laminin (green) and nuclei (DAPI, blue) on cryosection of muscles treated as in (B). On the right, the graph shows the percentage of IgG+ fibers/ total amount of fibers of muscles displayed on the left.. Data are represented as average ± SEM and statistics assessed by t-test (N=4). **D)** quantification of the levels (U/L) of serum creatine kinase by colorimetric assay. Data are represented as average ± SEM; statistics assessed by t-test (N=4).

G9a/GLP inhibitors have beneficial effects at late stages of DMD progression

In light of the results observed with young mdx mice we decided to test the impact of KMTis at later stages of DMD progression, when dystrophic muscles are already degenerated. To this end, we treated old mdx mice (12 months) for 45 days by daily intraperitoneal injection of A-366 and M108 and we then assessed muscles by histological evaluation (Fig7A).

Through immunofluorescence for collagen3A1 and Laminin on cryosections of TA, we demonstrated that both A-366- and M-108- treated mice showed an increased CSA and a reduced fibrotic infiltration, as compared to control animals (Fig.7B-C). Moreover, inspection of adipogenic infiltration revealed a decrease in the Oil Red O and perilipin positive area in KMTis-treated muscles, as compared to controls (figure 7D-E). Further, quantification of the percentage of Myeloperoxidase (MPO) positive cells demonstrated a reduction of inflammatory infiltration in KMTis-treated muscles, as compared to controls (figure 7F).

Overall, our data demonstrated that G9a/GLP inhibition exerts beneficial effects on dystrophic muscles at later stages of DMD progression, in which adipogenic and inflammation contents are the prominent side effects of dystrophin absence and in which the muscle environment is exacerbated by chronic damage.

Of note, the evidence that G9a/GLP inhibition is beneficial at this stage indicates that these KMTs might represent more relevant pharmacological targets than HDACs, since we previously demonstrated that HDACi-mediated beneficial effects are instead restricted at early stages of DMD (Mozzetta et al., 2013) and they are not effective when administered once DMD is already exacerbated.

Figure 7

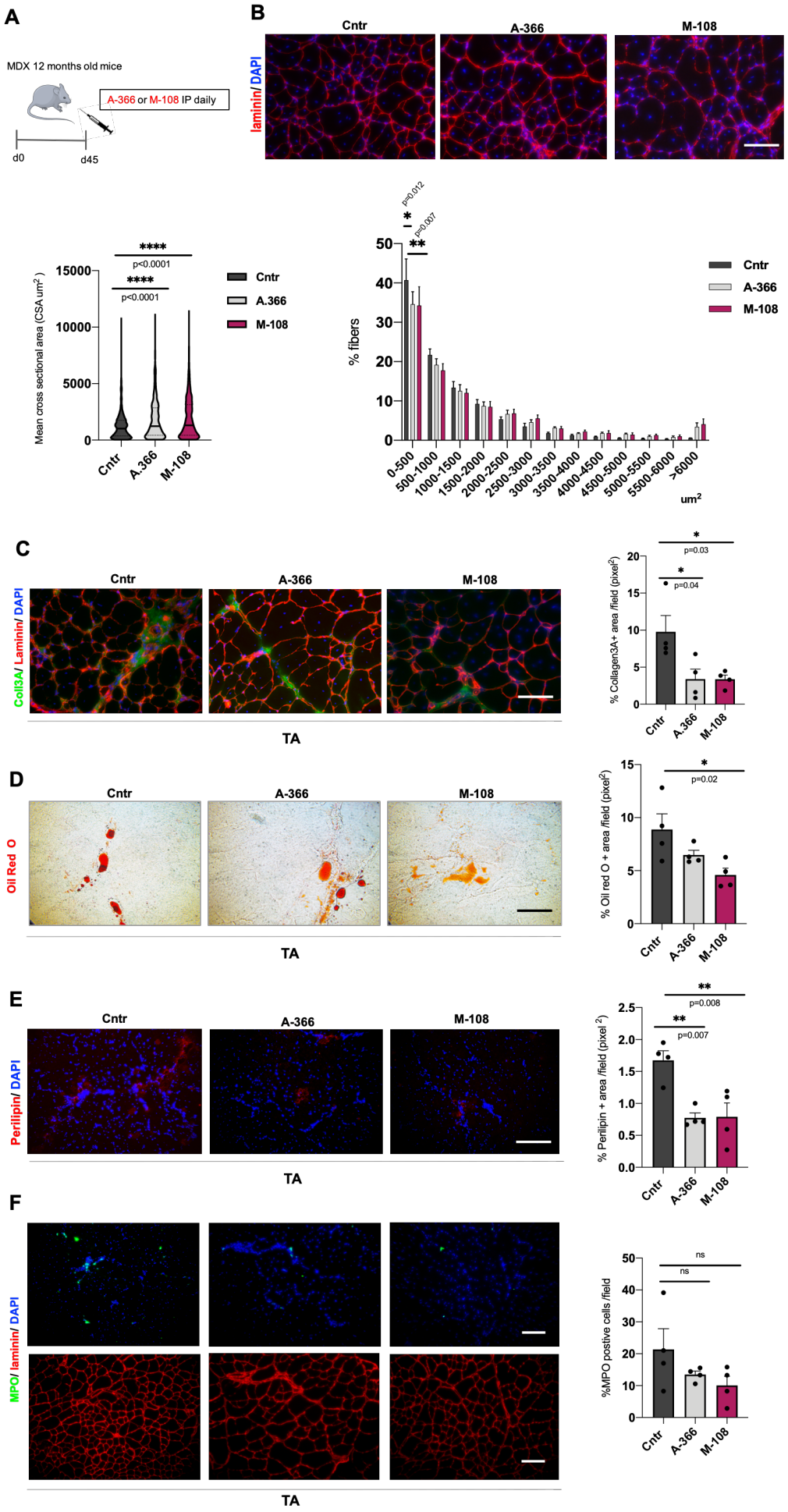
A
MDX 12 months old mice
A-366 or M-108 IP daily
d0
d45
B
Cntr
A-366
M-108
laminin/ DAPI
Mean cross sectional area (CSA um²)
****
p<0.0001
****
p<0.0001
Cntr
A.366
M-108
% fibers
p=0.012
p=0.007
0-500
500-1000
1000-1500
1500-2000
2000-2500
2500-3000
3000-3500
3500-4000
4000-4500
4500-5000
5000-5500
5500-6000
>6000
um²
C
Coll3A/ Laminin/ DAPI
TA
% Collagen3A+ area /field (pixel²)
p=0.03
p=0.04
D
Oil Red O
TA
% Oil red O + area /field (pixel²)
p=0.02
E
Perilipin/ DAPI
TA
% Perilipin + area /field (pixel ²)
p=0.008
p=0.007
F
MPO/ laminin/ DAPI
TA
%MPO postive cells /field
ns
ns

Figure 7: G9a/GLP inhibitors have beneficial effects at late stages of DMD progression. A) Scheme of the experiment. **B)** *Upper panels:* IF for laminin (red) and nuclei (dapi, blue) on cryosections of TA isolated from old mdx mice treated with KMTis for 45 days (see scheme). *Lower panels:* violin plot showing distribution of single myofibers CSA, statistics by One-way Anova (left)*:* % of myofibers with CSA within the shown ranges (*right)*. Data are represented as average ± SEM (n=4), statistical significance assessed by Two-way Anova. **C)** IF for Collagen3A (green), laminin (red) and nuclei (dapi, Blue) on cryosections of TA from mdx mice treated as in (A). On the right the graph shows quantification of the % of Collagen3a+ area. Data are represented as average ± SEM; (n=4). Statistical significance assessed by One-way Anova. **D)** Staining for Oil Red O of muscles from mice treated as in (A) and graph showing quantification of the ORO+ area on the right. Data are represented as average ± SEM; (n=4). Statistical significance assessed by one-way Anova. **E)** Representative images of the same TA muscles shown in D) stained for perilipin (red), another adipogenic marker, and nuclei (dapi, blue). On the right, the graph shows the percentage of perilipin stained area. Data are represented as average ± SEM; (n=4) Statistical significance assessed by one-way Anova. **F)** IF for Myeloperoxidase (MPO; green), laminin (red) and nuclei (dapi, blue) on TA muscles mice treated as in (A). The right graph shows quantification of the percentage of MPO positive cells / field (n=4). Data are represented as average ± SEM. Statistical significance assessed by one-way Anova.

G9a and GLP are involved in specific repression of FAPs transcriptional programs and A-366 treatment induces acquisition of alternative fate

Stage-specific beneficial effects of HDACi are mediated by FAPs, since their restricted chromatin malleability limits the capacity of HDACi to unlock FAPs' chromatin of pro-myogenic loci (Mozzetta et l., 2013; Saccone et al., 2014). In light of the efficacy of G9a/GLP inhibitors also in old dystrophic mice, we hypothesized that G9a/GLP might represent the epigenetic constraints that limit FAPs susceptibility to epigenetic drugs. In line with this idea, we observed that G9a/GLP are mainly expressed in FAPs, as compared to MuSCs, and become particularly enriched in FAPs from old (late-stage) dystrophic muscles (Fig.8A). These results led us to speculate that G9a and GLP are involved in specific epigenetic repression of FAPs trascriptional programs at advanced stages of the disease. To provide evidence in this direction, we performed RNAseq analysis in FAPs from young and old mdx mice (Fig.8B-C). We could find 315 genes differentially expressed (DEGs), among which the majority (244) were down-regulated (Fig. 8C), in agreement with an increased presence of G9a/GLP and its associated repressive mark (H3K9me2) (Fig.8A). Moreover, Gene set enrichment analysis (GSEA) (Fig.8D) and Gene Ontology (GO) (Fig.8E) highlighted that downregulated genes are mostly associated to mitosis and cell cycle progression. These results suggest that old dystrophic FAPs have an impaired proliferation capacity. To test if this inability might be overcome by the inhibition of G9a/GLP, we then assessed the percentage of proliferating FAPs isolated both from control and A366-treated mdx mice. Of note, IF for Ki67, a marker of actively dividing cells, revealed that A366 treatment increased the proliferative capacity of FAPs (Fig.8F). This boost in proliferative potential was also confirmed *in vivo* (Fig. 8G), since muscles from A-366 treated mice displayed a higher percentage of total FAPs (Sca1+) and proliferating FAPs (double positive for Sca1 and Ki67). Since A366-treated muscles show reduced fibrotic infiltration, we believe that accumulation of FAPs might be instead beneficial to maintain a subpopulation of pro-myogenic FAPs that promote MuSCs-mediated regeneration while also participating directly to myogenesis.

In fact, inhibition of G9a/GLP induces them to choose alternative fates (i.e.myogenic) instead of the fibro-adipogenic one (Biferali, Bianconi et al., *under revision*). In agreement with this, analysis of *ex vivo* culture of FAPs isolated from 14 days A-366 treated mdx mice, revealed that FAPs could form MyHC positive myotubes in differentiation media, at the expenses of the accumulation of adipocytes, as compared to FAPs from control mice (Figure 8 H-I). Overall,

our data led us to speculate that the administration of such epigenetic drugs might increase FAPs developmental capacities, overcoming the epigenetic “barrier” of repression by de-repressing silent transcriptional programs and ultimately leading them to acquire alternative (i.e. myogenic) cell fates.

Figure 8

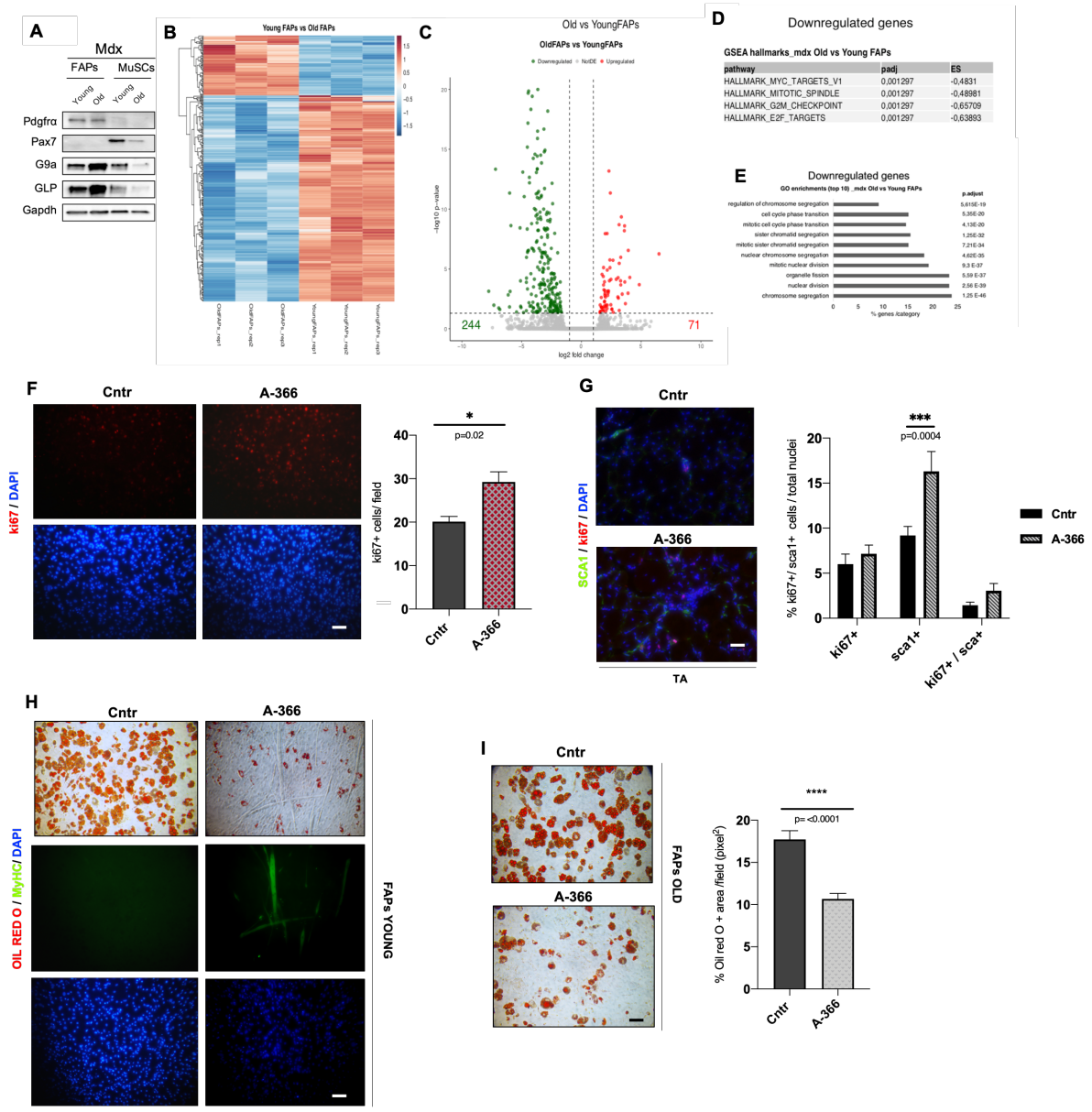

Figure 8: G9a and GLP are enriched in FAPs from old dystrophic muscles and limit their proliferative and myogenic capacity. A) Western blot analysis of young and old FAPs, as compared to young and old MuSCs, both isolated from mdx mice. **B-C)** Young vs Old FAPs RNAseq Heatmap (B) and Volcano plot (C) showed the extent of down- and up-regulated transcripts among the differentially regulated genes (DEG), defined by a minimum fold change difference of 2 (1<log2FC<1) and an adjusted p value<0.05. **D)** Gene Set Enrichment Analysis (GSEA) of down-regulated genes revealed hallmarks associated with different pathways involved in cell cycle progression. **E)** The top 10 Gene Ontology (GO) categories among the downregulated genes. **F)** IF for ki67 (red) of young mdx FAPs isolated from control and *in vivo* A366-treated mice for 14 days. Nuclei were counterstained with dapi (blue). Quantification of the % of Ki67+ cells/field is shown on the right. Data are represented as average ± SEM. Statistical significance assessed by t-test (n=3)**. G)** IF on TA muscles, from mdx mice treated for 45-days with A366, for Sca1 (green), KI67 (red) and nuclei in dapi (blue) and its quantification (graph on the right) (n=5). Data are represented as average ± SEM. Statistical significance assessed byTwo-way anova. **H)** FAPs isolated from young mdx mice treated with A-366 for 14 days.

Oil Red O staining (*upper panels)* and IF for MyHC (green) and DAPI (blue) (*Lower panels)*. **l)** FAPs isolated from old mdx mice treated with A-366 for 14 days; Oil Red O staining and quantification of ORO+ area (n=3). Data are represented as average ± SEM. Statistical significance assessed by t-test**.**

HDAC class I inhibition induce morphological recovery of dystrophic muscles

HDACis have been already tested in different skeletal muscle pathologies and in particular in muscular dystrophies. To bypass the limits of the specificity of HDACi, we decided to test a new class I HDACi (HDACi-I) (Bresciani et al., 2018) in order to improve the selectivity and the efficacy of these kind of molecules. In collaboration with IRBM, we tested in a 105 days long treatment a new HDAC-I (I-209) in dystrophic mice (8 weeks old) and we used Givinostat (I-192) as positive control of efficacy (Consalvi et al., 2013). We administered orally (by gavage), the class I HDACi, daily in two doses (fig.9A). We collected blood every 30 days to check levels of serum Creatine Kinase (CK). The levels calculated by the assay (Fig.9B) showed a statistically significant variation, between the groups treated with the two doses of Class I HDACis compared to the control group on day 23, and in all experimental groups decrease over time as a sign of stabilization of DMD symptoms, typical of the mdx mouse. We performed histological analysis on TA isolated from each experimental group. The results obtained by this experiment show that inhibition of class I HDAC increased myofibers' area (Fig.9C-D) and diameter (Fig.9E), to levels comparable to those observed for Givinostat (I-192). We then evaluated adipogenic infiltration by Oil red O staining and observed a reduction of adipogenic deposition with the two different doses of class I inhibitor (fig. 10A). This was paralleled by a decrease of collagen 3A deposition, both on hindlimb skeletal muscles (TA) and diaphragm (fig.10B-C).

Moreover, class I HDACs inhibition displayed a protective role on dystrophic muscles since prevented accumulation of inflammation and myofibers necrosis. Indeed, analysis of MPO accumulation by IF showed that both doses of class I HDACi, are able to reduce the inflammation and the release of myeloperoxidase in the site of injury during the degenerative phase (fig.10D). Finally, the necrosis that characterized the fibers' in dystrophic skeletal muscle diminished upon treatment with HDACis compound, highlighted by a decrease of myofibers' positive for IgG (fig10E). Taken together, these data demonstrate that specific inhibition of class I HDACs is able to exert the same beneficial effects observed by pan-HDACs inhibition emphasizing that improving selectivity does not affect efficacy.

Figure 9

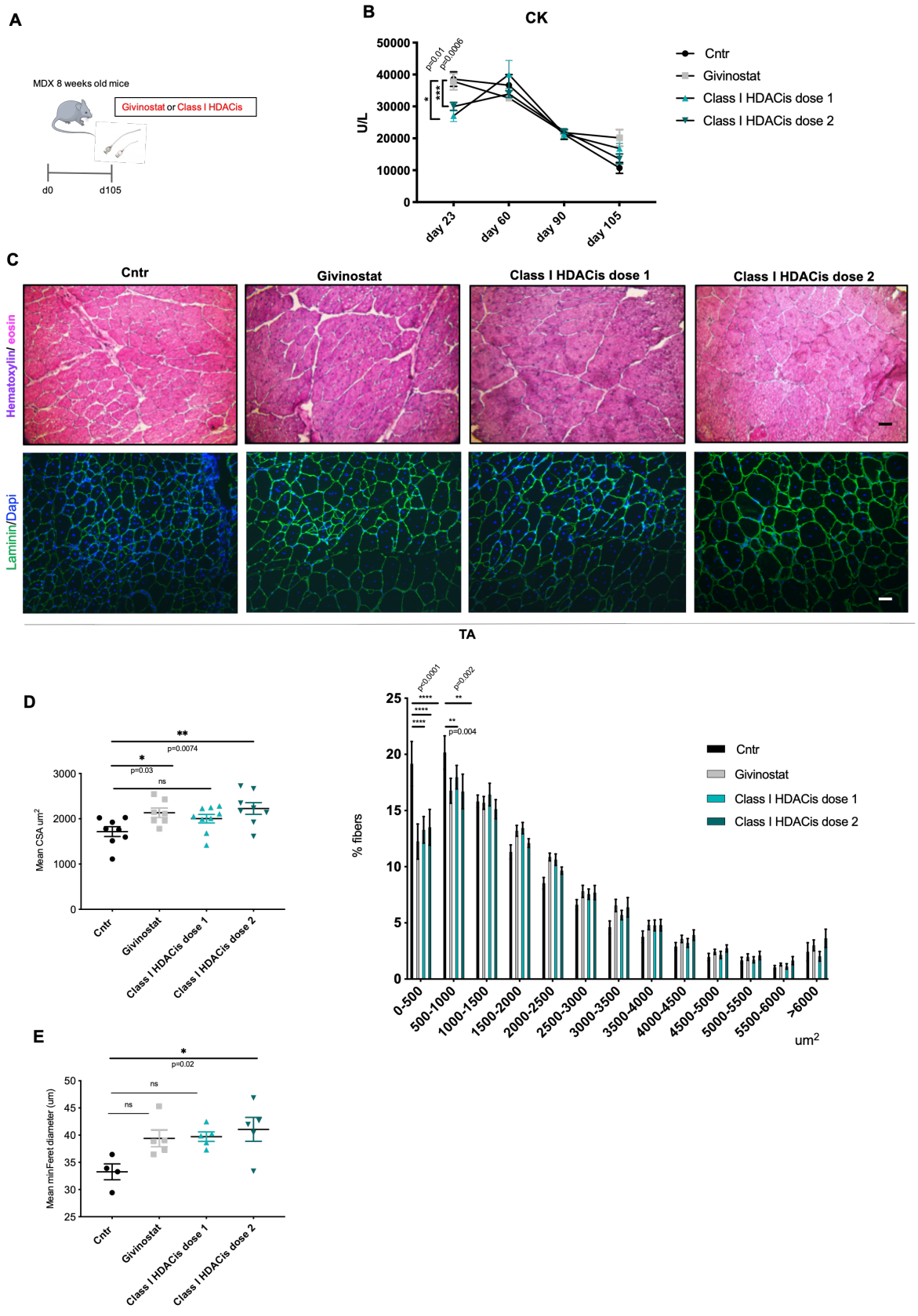
A
MDX 8 weeks old mice
Givinostat or Class I HDACis
d0
d105
B
CK
U/L
p=0.01
p=0.0006
Cntr
Givinostat
Class I HDACis dose 1
Class I HDACis dose 2
day 23
day 60
day 90
day 105
C
Cntr
Givinostat
Class I HDACis dose 1
Class I HDACis dose 2
Hematoxylin/ eosin
Laminin/Dapi
TA
D
Mean CSA um2
p=0.0074
p=0.03
ns
E
Mean minFeret diameter (um)
p=0.02
% fibers
p<0.0001
p=0.002
p=0.004
um2

Figure 9: HDACs class I inhibition induces morphological recovery of dystrophic muscles.
A) Representative scheme of 105 days long study with mdx mice treated every day by gavage with vehicle (CNTR), Givinostat or class I HDACis in two different doses. **B)** Evaluation of the serum CK levels (U/L) in blood collected from mdx mice treated as in (A). Data are represented as average ± SEM. (n=4). Statistical significance assessed by two-way Anova. **C)** Hematoxilin/eosin staining (*upper panels)* and IF for laminin (green) and nuclei (dapi; blue) (*lower panels*) on cryosections of tibialis anterior from mice treated as described in (A). **D)** Graphs show the mean CSA (left) and the distribution of the percentage of fibers' caliber (right). Data are represented as average ± SEM; (n=8). Statistical significance assessed by one-way Anova for mean CSA and two-way Anova for fibers distribution. **E)** The graph shows the minimum feret's diameter. Data are represented as average ± SEM; (n=5) Statistical significance assessed by one-way Anova.

Figure 10

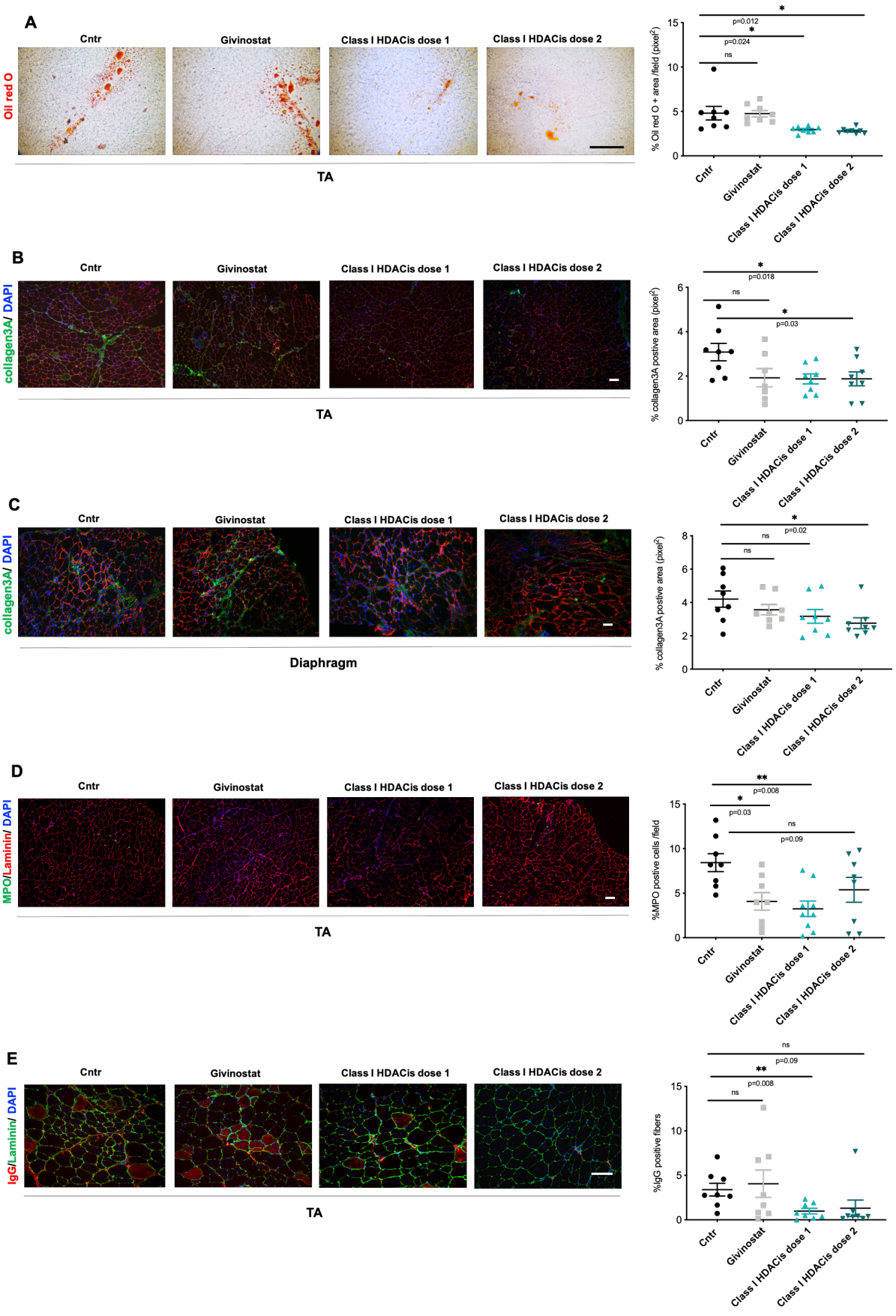
A
Cntr
Givinostat
Class I HDACis dose 1
Class I HDACis dose 2
Oil red O
TA
% Oil red O + area /field (pixel²)
p=0.012
p=0.024
ns
B
collagen3A/ DAPI
% collagen3A postive area (pixel²)
p=0.018
p=0.03
C
Diaphragm
p=0.02
D
MPO/Laminin/ DAPI
%MPO postive cells /field
p=0.008
p=0.03
p=0.09
E
IgG/Laminin/ DAPI
%IgG positive fibers

Figure 10: HDAC class I inhibition induces morphological recovery of dystrophic muscles. A) Staining for Oil Red O (ORO) of TA muscles isolated as described in figure 9. The graph on the right shows the % of ORO+ area as pixel^2/field. Data are represented as average ± SEM. Statistical significance assessed by one-way Anova (n=8). **B-C)** IF for Collagen3A (green), laminin (red) and nuclei (dapi, blue) on cryosections of TA (B) and diaphragm (C) from mdx mice treated as described in Fig. 9A. On the right, graph shows the percentage of the collagen3A+ area as pixel^2/field. Data are represented as average ± SEM. Statistical significance assessed by one-way Anova (n=8). **D)** IF for myeloperoxidase (MPO; green), laminin (red) and nuclei (dapi; blue) ton TA from mice treated as in Fig.9A. The extent of inflammation was evaluated as percentage of MPO+ cells/field, as show in the graph on the right. Data are represented as average ± SEM. Statistical significance assessed by one-way Anova (n=8). **E)** IF for IgG (red), laminin (green) and dapi (blue) to highlight necrotic fibers, quantified as the percentage of IgG+ fibers for field. Data are represented as average ± SEM. Statistical significance assessed by one-way Anova (n=8).

Class I HDAC inhibition induces macrophages polarization towards an anti-inflammatory phenotype

Following the analysis of myeloperoxidase, we decided to investigate more in depth the anti-inflammatory potential of class I HDACi, as inflammation is responsible for the exacerbation of muscle damage in DMD. In fact, macrophages contribute to muscle wasting also promoting inflammation-mediated necrosis. For this reason, we decided to analyze the status, and amount, of macrophages, taking advantage of the different markers able to highlight the anti-inflammatory phenotype (i.e. CD206), known as M2, which also supports the differentiation of muscle stem cells (Tidball 2017; Tidball et al., 2018), as compared to the pro-inflammatory phenotype, called M1, which is instead detrimental for muscle regeneration.

By immunofluorescence for F4/80 and CD206 (Fig.11 A-B), we observed a decrease in the total content of macrophages (F4/80+), but an increase in the percentage of CD206+ cells, a marker of the M2 macrophages.

Figure 11

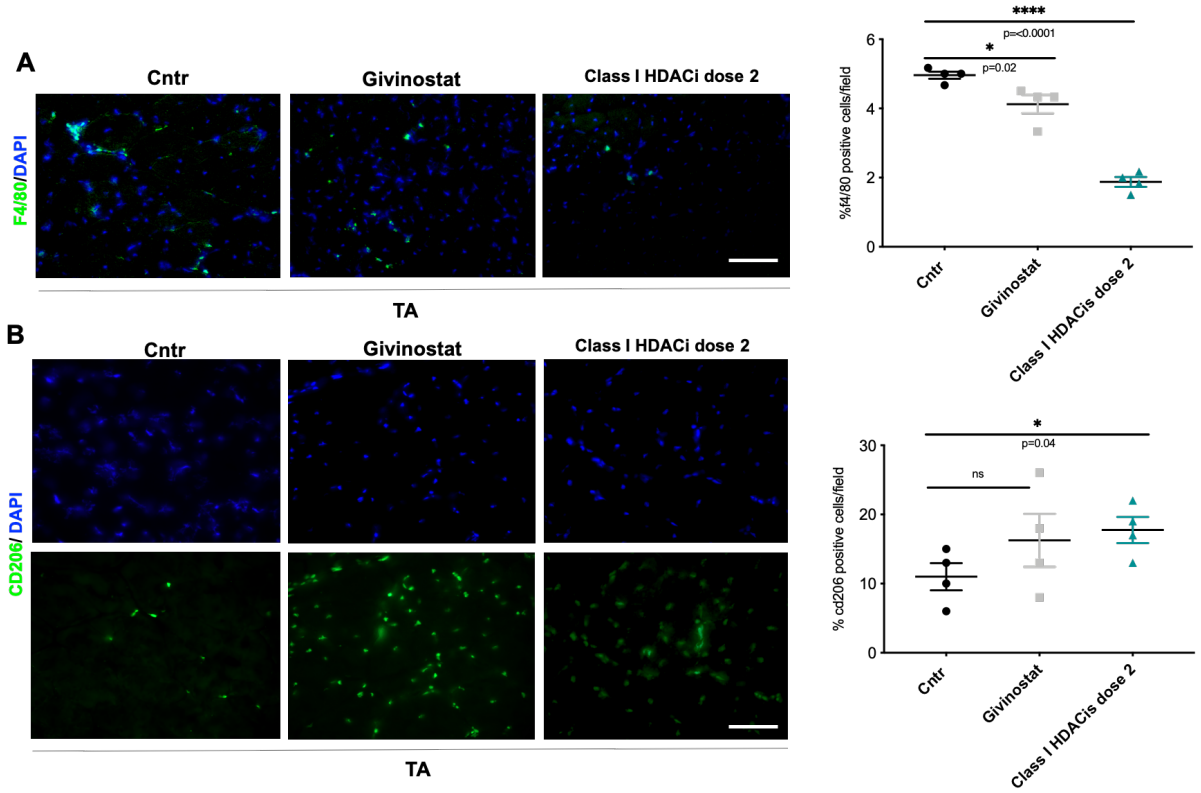

Figure 11: Class I HDAC inhibition induces macrophages polarization towards an anti-inflammatory phenotype. A) IF on TA muscles from mice treated as in Fig. 9A for F4/80 (green) and nuclei (DAPI, blue); the right graph shows the mean percentage of F4/80 + cells/field (n=4). Data are represented as average ± SEM. Statistical significance assessed by one-way Anova. **B)** IF for CD206 (green) and nuclei (DAPI, blue) on TA muscles from mice treated as in Fig. 9A. The right graph represents the quantification of the amount of CD206+ cells/field. Data are represented as average ± SEM; (n=4). Statistical significance assessed by one way Anova.

Class I HDAC inhibition induces FAPs expansion and acquisition of myogenic traits

We then analyzed the amount of FAPs by performing IF for PDGFRalpha (figure 12A) a specific marker for FAPs in skeletal muscle. Inhibition of class I HDACs induced an increase of PDGFRa+ cells, which is reminiscent of what we observed with G9a/GLP inhibitors, a result that together with the reduction of collagen and adipose infiltration observed in HDACi treated mice suggest that HDACi treatment induces an increase in a subpopulation of pro-myogenic FAPs.

In support of this idea, FAPs from mice treated *in vivo* with the pan-HDACi Givinostat and class I-HDACi acquired the capacity to form myotubes (Fig.12B) and to express the muscle-specific marker MyhC (Fig.12C, lower panel). Importantly, the acquisition of the myogenic capacity was paralleled by an impaired fibro- adipogenic differentiation, assessed by decreased levels of collagen3A1 (Figure 12C, lower panel) and a diminished number of adipocytes (Fig.12D), respectively. Intriguingly, Givinostat induced an overall reduction of H3K9me2 global levels in FAPs (Fig. 12C, upper part), suggesting a common epigenetic regulatory axis converging on H3K9 methylation and implying that the beneficial effects induced by pan-HDACi might be indirectly linked to modulation of H3K9 methylation.

Figure 12

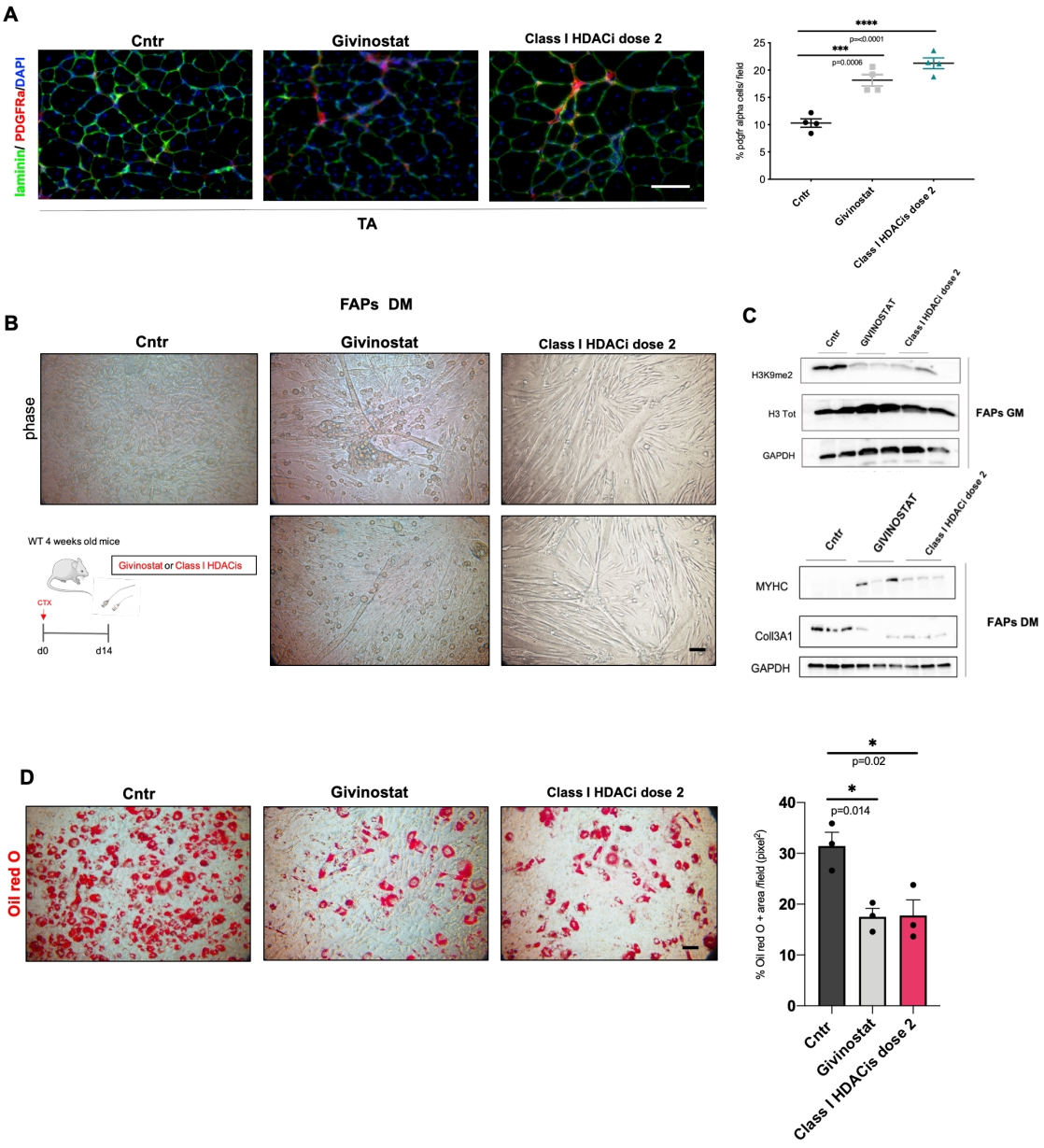

Figure 12: Class I HDAC inhibition induces FAPs expansion and acquisition of myogenic traits.
A) IF for PDGFRa (red), laminin (green) and nuclei (DAPI, blue) in TA muscles from mice treated as in Fig. 9A. The quantification is shown on the right as mean percentage of PDGFRa+ cells/field (n=4). Data are represented as average ± SEM and statistical significance assessed by one way Anova.
B)Phase-contrast images of FAPs isolated from injured wild type mice, treated with Givinostat and class I HDACis for 14 days mice treated as described in scheme and cultured ex-vivo in the absence of any treatment. **C)** Representative western blot of FAPs isolated from mice treated as described in (A), and cultured in growth (upper panels) or differentiation (lower panels) media. **D)** Oil Red O staining of FAPs cultured in adipogenic differentiation medium and its quantification shown as the percentage of the red oil O stained area as pixel^2/field, calculated with ImageJ software. Data are represented as average ± SEM. Statistical significance assessed by one way Anova (n=3).

Discussion

The pathogenesis of Duchenne Muscular Dystrophy (DMD) entails an initial compensatory regenerative response, followed by replacement of muscle tissue with fibrotic and fatty infiltrate. As a genetic disease, the cure for DMD would be the systemic introduction of the dystrophin gene into muscles of DMD boys, but unfortunately application of gene and cellular therapies is still far from the clinical practice (Gawlik et al., 2018). For this reason, pharmacological approaches that act downstream the genetic defect aimed to sustain a regenerative response are the most promising to at least prevent disease progression.
Epigenetic therapies are able of promote an efficient regenerative response of DMD muscles, while preventing fibro-adipogenic infiltration (Mozzetta et al. 2009). Previous works have already showed pre-clinical efficacy of epigenetic drugs in murine models of DMD, demonstrating that the use of pan_HDACi induces functional and morphological recovery of dystrophic muscles (Minetti et al 2006, Colussi et al., 2008; Consalvi et al 2013). These evidences provided a proof of principle that targeting chromatin modifiers might be a useful approach to promote the regenerative potential of muscle progenitor cells by inducing the transcriptional activation of the myogenic program (Iezzi et al 2004, Minetti et al 2006, Colussi et al., 2008, Mozzetta et al 2013). Other chromatin modifying enzymes, such as histone methyltransferases (KMTs) are emerging recently as key epigenetic players that dynamically control muscle genes expression. In particular, the H3K9 KMTs G9a and GLP are emerging as critical transcriptional regulators during myogenesis (Sartorelli and Juan, 2011). Thus, we reasoned that modulation of their activity by specific pharmacological inhibitors (KMTi) could represent a way to unlock the expression of muscle-specific genes and enhance muscle differentiation in pathological condition, such as DMD.

Here we report the first application of G9a/GLP inhibitors in murine models of DMD and skeletal muscle regeneration. Our experiments in murine models of necrosis-induced regeneration (CTX-induced injury) and DMD (mdx mice) demonstrate that *in vivo* treatment with G9a/GLP-specific inhibitors is effective in reducing methylation levels on whole skeletal muscles and on the populations involved in regeneration/degeneration processes, such as FAPs and MuSCs. Our results show that the reduction of H3K9 methylation is then translated into the promotion of satellite cells differentiation and, at the whole muscle level, of regeneration. In particular, satellite cells from KMTis-treated regenerating muscles showed an advantage in proliferation, which then led to an acceleration of their differentiation. This effect we believe is the one of the cause of the improved regeneration observed in the muscles of KMTis-treated mice. Indeed, in the experimental paradigm of CTX-induced regeneration, A-366-treated muscles displayed an increased myofibers area (CSA) accompanied by a decreased percentage of eMyHC+, immature, fibers, suggesting an overall acceleration of muscle regeneration.
Of note, FAPs isolated from A366-treated injured muscles showed an impaired adipogenic capacity. FAPs have been defined as bi-potent muscle-resident progenitors capable to differentiate *in vitro* and *in vivo* in fibroblasts and adipocytes (Joe et al., 2010; Uezumi et al., 2010). During skeletal muscle regeneration, FAPs quickly proliferate and expand, prior to satellite cells, providing a transient favorable environment to promote satellite cell-mediated regeneration (Heredia et al., 2013; Joe et al., 2010). The effect obtained with A366 treatment suggests that the activity of FAPs is malleable as the inhibition of H3K9 methyltransferases induced them to choose alternative fates (i.e.myogenic) instead of the fibro-adipogenic one. We speculate that the administration of such epigenetic drugs might lead to the modification of FAPs transcriptional programs ultimately affecting cell fates. This hypothesis is supported by the effect we observe in inhibiting the deposition of adipose and fibrotic tissue in the total

muscle, on a model of chronic degeneration such as mdx mice. Indeed, G9a/GLP inhibition prevents fibrotic and fat infiltration in dystrophic muscles. This evidence, together with the data showing that FAPs isolated from KMTi-treated muscles display reduced adipogenic differentiation together with the acquisition of the competence to form myogenic differentiated cells support the idea that G9a/GLP inhibitors might exert their beneficial effect also by modulating the fate of dystrophic FAPs. This is in agreement with our data demonstrating that G9a/GLP methyltransferases cooperate with Prdm16, a FAPs-enriched factor that targets H3K9me2 at muscle-specific loci at the nuclear periphery (Biferali, Bianconi et al*., under revision*).

In particular, we speculate that these enzymes restrict FAPs developmental plasticity in FAPs along DMD progression. In support of this hypothesis, we found G9a/GLP mainly expressed in FAPs isolated from mdx mice at advanced stages of DMD (old). Moreover, transcriptional profiling revealed that old FAPs have a higher number of repressed genes enriched within categories belonging to mitosis and cell cycle regulation, suggesting that higher levels of epigenetic repressors such as G9a/GLP might restrain FAPs regenerative and proliferative capacities. Importantly, A-366 treatment triggered a boost in FAPs proliferation, forcing them towards the myogenic program. Taken together, these data suggest that the activity of FAPs is malleable and the epigenetic inhibition of H3K9me2 might confer them the capacity to choose alternative fates instead of the fibro-adipogenic one. This hypothesis needs certainly further validation, but our data realistically point towards G9/GLP being responsible of the epigenetic barrier that silences their pro-myogenic fate. In support of our idea, we found that administration of KMTis to old mdx mice at advanced stages is sufficient to exert beneficial effects, suggesting that erasure of H3K9 methylation might promote pro-regenerative response also in degenerated muscles. This evidence underscores the potential of KMTi in the treatment of DMD at advanced stages, when instead other epigenetic drugs (i.e. HDACi) are no longer effective (Mozzetta et al., 2013).

Pro-regenerative effect obtained in dystrophic mice through treatment with these novel KMTs inhibitors highlight the therapeutic potential of more selective compounds as an approach to increase efficacy, safety and tolerability of epigenetic therapy in DMD. This notion, promoted our interest in testing also HDACi compounds specific for class I. Our results showed that inhibition of even one class of HDACs is sufficient to obtain beneficial effects on skeletal muscle. Treatment of dystrophic mice with class I HDACi (developed and provided by our collaborators at IRBM) leads to an increased caliber of myofibers and slow down the deposition of adipose tissue, a typical detrimental effect of the progression of DMD. Moreover, class I HDACs inhibition leads to a reduction in inflammation and muscle necrosis, inducing polarization of macrophages towards an anti-inflammatory phenotype thus suggesting that the use of these more selective drugs might protect against muscle degeneration.

The use of more specific Class I HDACs inhibitors could provide a valuable tool to bypass not only the lack of selectivity of the current inhibitors but also to increase their effectiveness, providing improvement in functional results that are not evident with current treatments. In fact, although the first clinical trial with pan-HDACi Givinostat in ambulant DMD boys showed beneficial effect on morpho-histological parameters, it did not exert amelioration of functional parameters.

Finally, we showed that Givinostat induced an overall reduction of H3K9me2 global levels in FAPs, this observation leads to the intriguing speculation that the beneficial effects observed by either HDACs and H3K9 KMTs inhibitors, might be commonly mediated by the reduction of H3K9 methylation levels, through a yet unknown mechanism.

Taken together, the results obtained during my PhD project revealed novel epigenetic targets that could be further exploited to unlock the expression of muscle-specific genes and to enhance muscle differentiation in pathological condition, such as DMD and they might even serve as a basis to conceive future combined therapies targeting both HDACs and KMTs.

Methods

KEY RESOURCES TABLE

REAGENT OR RESOURCE	SOURCE	IDENTIFIER CODE
Experimental model/ *in vivo* procedure		
TEKLAD RODENT DIET	ENVIGO	N.A.
ISOFLUORANE ISO-VET 1000mg/g	PIRAMAL	104331020
C57/BL6J MICE	JACKSON LABORATORY	N.A.
C57BL/10ScSn-Dmdmdx/J	JACKSON LABORATORY	N.A.
micro-fine 0,5ml/0,8ml insulin 30G X8mm	BD	324825
Plastic feeding tubes, 20ga x 30mm	INSTECH	FTP-20-30
Plastic feeding tubes, 18ga x 30mm	INSTECH	FTP-18-30
cardiotoxin	LAXOTAN	L8102
(2-Hydroxypropyl)-β-cyclodextrin POWDER	SIGMA	H107
Cells colture		
CYTOGROW	RESNOVA	9001-B
ECM GEL	SIGMA	E1270
PBS	SIGMA	D8537
DMEM	SIGMA	D5671
FBS, CERT, USA ORIGIN	GIBCO	16000044
HORSE SERUM HEAT INACTIVATED	GIBCO	26050088
multiwell 24	FALCON	FC-1353047
INSULIN	SIGMA	I9278

FACS		
ANTI MOUSE Ly-6A E (SCA-1) FITC	MILTENYIBIOTEC	130-116-490
ANTI-MOUSE CD45 PE	MILTENYIBIOTEC	130-110-707
ANTI-MOUSE TER-119 PE	MILTENYIBIOTEC	130-112-909
ANTI-MOUSE CD31 (PECAM-1) PE	MILTENYIBIOTEC	130-111-540
ANTI-INTEGRIN ALPHA7 APC VIO770	MILTENYIBIOTEC	130-102-719
Dispase II	ROCHE	04 942 078 001
COLLAGENASE A	ROCHE	10103586001
DNAse I	ROCHE	1284932
CaCL2	APPLICHEM	A3652
MgCl2	APPLICHEM	A4425
HBSS, W/O PHENOL RED	GIBCO	14025100
ANTIBODIES IF/WB		
ANTI-LAMININ ANTIBODY	SIGMA	L9393
ANTI-PERILIPIN ANTIBODY	SIGMA	P1873
ANTI-MYHC (Mf20)	DSHB	mf20-s
ANTI MYHC3	DSHB	F1.652-s
ANTI- HISTONE H3 DYMETIL K9	ABCAM	1220
ANTI-HISTONE H3	ABCAM	10812
ANTI- KI67	ABCAM	AB15580
ANTI-COL3A1	SANTA CRUZ	SC271249
ANTI- PDGFR ALPHA	R&D	AF1062
ANTI-MYELOPEROXIDASE	R&D	AF36667
ANTI F4/80 FITC	BIORAD	MCA497FA
ANTI CD206 FITC	BIOLEGEND	141704
FAB goat anti mouse IgG	AFFINIPURE JACKSON	JI115007003

Biotin-SP Goat Anti-Mouse IgG	AFFINIPURE JACKSON	JI115065205
Cy3-Streptavidin	AFFINIPURE JACKSON	JI016160084
ALEXA ANTI RABBIT 488	THERMO FISHER	a21206
ALEXA ANTI MOUSE 488	THERMO FISHER	A21202
ALEXA ANTI RABBIT 594	THERMO FISHER	A21207
ALEXA ANTI MOUSE 594	THERMO FISHER	A21203
ANTI-RABBIT IgG	SIGMA	A9169
ANTI-MOUSE IgG	SIGMA	A9044
ANTI-GAPDH	SIGMA	G9545
CHEMICALS/REAGENTS		
paraformaldehyde	SIGMA	P6148
ETHANOL	SIGMA	0-2860
Acetone	SIGMA	32201
0-XYLENE	SIGMA	X1040
PICRIC ACID	SIGMA	P6744
HCL	SIGMA	H1758
GLYCEROL	APPLICHEM	A2926 0500
METHANOL	SIGMA	34860
BSA	SIGMA	A2153
ACETIC ACID	SIGMA	27221
SKIM MILK	SIGMA	70166
BOUIN'S SOLUTION	SIGMA	HT10132
triton X100	SIGMA	T8787
2-Methylbutane	SIGMA	320404
Sodium chloride NaCl	APPLICHEM	A2942
EDTA	SIGMA	A1104

TWEEN	APPLICHEM	A1389
TRIZMA	SIGMA	T1503
DAPI	SIGMA	D9542
ACRYLAMIDE/BIS-ACRYLAMIDE, 30%	SIGMA	A3574
AMMONIUM PERSULFATE ELECTROPHORESIS	SIGMA	A3678
Phenylmethanesulfonyl fluoride solution	SIGMA	93482
ISOPROPANOL	SIGMA	I9516
BCA PIERCE KIT	THERMO scientific	23225
SUPER SIGNAL WEST DURA	THERMO scientific	34075
creatine kinase activity assay kit	ABCAM	ab155901
complete protease inhibitors tablets	ROCHE	0-4693116001
DNASE I	THERMO scientific	EN0521
HISTOLOGY MATERIAL		
HEMATOXYLIN	SIGMA	HHS32
EOSIN Y SOLUTION	SIGMA	HT110332
RED OIL O	SIGMA	O0625
SIRIUS RED F3B	SIGMA	35782
EUKITT	SIGMA	0-3989
CLICKIT EDU HCS ASSAYS	INVITROGEN	10354
Tissue tek cryomold	SAKURA	4566
OCT RESIN	SAKURA	4583
SUPERFROST GLASS	THERMO FISHER	J4800AMNZ
INSTRUMENTS/SOFTWARE		
CHEMIDOC	BIORAD	XRS+
CRYOSTAT	LEICA	CM-3050 S
MICROSCOPE	NIKON	eclipse TE300

MICROSCOPE	ZEISS	AXIO VISION III/ COLIBRI7
TISSUE RUPTOR	QUIAGEN	9001272
IMAGEJ SOFTWARE /FIJI	NIH	N.A.
IMAGELAB 6.0 SOFTWARE	BIORAD	N.A.
PRISM SOFTWARE	GRAPHPAD SOFTWARE	N.A.
FACS ARIA III	BD BIOSCIENCES	N.A.

Mouse models and *in vivo* treatments

For the experiments described in this study were used male C57/BL6J wild-type mice and male/female C57BL/10ScSn-*Dmd*^{mdx}/J purchased from Jackson Laboratories. All animal procedures were approved by the Institutional Animal Care and Use Committee of Dept. of Biology and Biotechnology of University Sapienza and were communicated to the Italian Ministry of Health and local authorities according to Italian law.
Mice were housed and maintained on a 12-hour light/ 12-hour dark cycle at constant temperature (22° +/-2°C), with a humidity between 50% and 60%, in animal cages with maximum 4 animals. Food and water were available ad libitum. For experiments with wild type mice, mice were anesthetized, and muscle injury was induced by intra-muscular injection of Cardiotoxin (CTX, Laxotan) 20 µg/ml dissolved in saline solution.

For *in vivo* KMT inhibitors experiments, we used 8 weeks old male wild type mice for 5 days long study and 8 weeks old and 12 months old male/female Mdx mice for the 45 days long treatments. Control vehicle solution (10% H-P-β-Cyclodextrin in Citrate Buffer), A-366 compound (from IRBM, dose 0,2 mg/kg or 2mg/kg in vehicle solution) or M-108 (from IRBM, dose 2mg/kg in vehicle solution) were administrated daily by intraperitoneal injection (IP). Vehicle solution and relative KMTis solutions were prepared fresh every day.

For *in vivo* HDACis experiments, we use 8 weeks old mdx mice for 105 days long treatment. All the treatments were administrated daily by oral gavage. Control animals were treated with vehicle solution (25%PEG 75%Water); the second group of animals was treated with Givinostat (from IRBM, in vehicle solution dose 5mg/kg); the third and fourth group of animals were treated with two doses of class I HDACi (from IRBM in vehicle solution) respectively with 0,5mg/kg and 1 mg/kg dose (indicated in the text as dose 1 and dose 2). Vehicle solutions and relative HDACis compounds were prepared fresh every day. For HDACis experiment in wild type mice, we use 4 weeks old mice for a 14 days long study; all the animals were treated daily by oral gavage. Control animals were treated with vehicle solution (25%PEG 75%Water); the second group of animals was treated with Givinostat (from IRBM, in vehicle solution dose 5mg/kg); the third group treated with class I HDACi dose 2 (from IRBM in vehicle solution, 1 mg/kg dose).

For functional studies, we used the guidelines in TreatNMD (treat-nmd.org); for hanging wire test, we used longest suspension time-method described in Protocol DMD_M.2.1.004. For treadmill test, we analyzed the total distance run by each mouse until exhaustion; we use guidelines in protocol DMD_M.2.1.001 and DMD_M.2.1.003, and the run parameters setting described in Consalvi et al., 2013.

Histological analysis and blood Collection

During KMTis treatment experiments, we collected blood from Mdx mice every 15 days (1h post injection) from retro-orbital plexus after Isolfuorane anesthesia (Iso-Vet 1000mg/g). During HDACis treatment experiments, we collected blood from Mdx mice every 30 days (1h post gavage) from retro-orbital plexus after Isolfuorane anesthesia (Iso-Vet 1000mg/g). Blood samples were centrifuge (at + 4 ° C, 2200g for 10 minutes) and evaluate the serum Creatine Kinase content with Creatine Assay kit (Abcam).

At the end of experiments, all animals were sacrified after anesthetized and dislocated. Hindlimb muscles (*tibialis anterior, quadriceps* and *grastrocnemius*) and diaphragm of all mice for each experiment were collected in cryomold (Sakura) and embedded in OCT (Sakura). The muscle in OCT is frozen in isopentane (Sigma), which is cooled by liquid nitrogen. Muscles are mounted on cryostat LEICA CM 3050S (at -20°C temperature) and cut in transversal cryosections of 8 µm.

Eosin/hematoxylin staining: the frozen sections were washed with PBS to re-hydrate them; cryosections were later fixed in paraformaldehyde (Sigma) at 4% for 10 minutes, washed in PBS (Sigma) and briefly in distilled water. Later, sections were stained in hematoxylin (100%, Sigma) for 8 min, washed in running tap water and later counterstain with eosin (100%, Sigma) and for 1 min. After a rinse in distilled water, the cryosections were dehydrated with increasing percentages of Ethanol (Sigma), fixed in o-Xylene (Sigma) and mounted with Eukitt medium (Sigma).

Red oil staining: the sections were washed with PBS to re-hydrate them. Later on, sections were fixed for 20 minutes with 4% paraformaldehyde. After washes with distilled water, sections were incubated with 60% isopropanol (Sigma) for 5 minutes. After completely air dry, incubate the sections for 10 minutes with red oil working solution (from powder Sigma, dissolving in isopropanol 100% and filtered). Red oil was removed from the sections and immediately replace with distilled water. After final washes, sections were mounted with glycerol (3: 1 in PBS) (Applichem).

Sirius red staining: as described in De Bruin et al., 2014, cryosections were fixed in 100% Acetone (Sigma) for 30 minutes and later incubated with bouin's solutions (Sigma) for 30 minutes at room temperature. Later on, sections are dyed with Picro-sirius solution (0,1% Sirius red F3B, Sigma, in picric acid, Sigma) in dark environment. After a brief wash in 10 mM HCl solution (in water, Sigma), sections were rinsed in 100% Ethanol twice, in o-Xylene once, and finally mounted with Eukitt (Sigma).

Immunofluorescence

After hydration of the slides with PBS, cryosections were fixed in 4% paraformaldehyde for 20 min. Later sections were fixed for 6 minutes in cold 100% Methanol (Sigma) at -20 ° C or, for cells, in 0,1% Triton X-100 at room temperature. After washing with PBS, slides are incubated with 4% BSA solution (Sigma) in PBS for a block of 1-3 hours. To reduce background, sections

are incubated with FAB goat anti mouse IgG (Affinipure Jackson, dilution 1:100). This step is avoided for IgG staining. Then, sections were incubated over night with primary antibody diluted in the block solution in a humidified chamber at + 4 ° C. Next day slides were washed in 0.1% BSA in PBS, and add the corresponding secondary antibody diluted in block solution for 1 hour at room temperature. After washes, slides were incubated with DAPI (Sigma) for 5 minutes. After a rapid wash, sections were mounted with glycerol (3: 1 in PBS, Applichem).
For F4/80 (Biorad) and CD206 (Biolegend) IF, cryosections, sections are not fixed. After permeabilization with 100% Acetone, they are air dried and then incubate with 4%BSA (Sigma); the incubation of primary antibodies is over night. After incubation with secondary antibody, the sections are counterstained in DAPI and mounted as describe above.
For EdU staining, we used Clickit EDU assay (Invitrogen).

Primary Antibody used: anti-laminin (Sigma) was used at the dilution 1:300; anti- H3 dymethil K9 (Abcam) 1:100; anti-eMyHC (DSHB) 1:20; anti-MyHC 1:100 (DSHB); anti-perilipin (Sigma) 1:200; anti-ki67 (Abcam) 1:200; anti-collagen 3A1 (Santa Cruz) 1: 200; anti-myeloperoxidase (MPO, R&D) dilution 1:100; anti-Pdgfr-alpha (R&D) 1:100. Anti-CD206 (Biolegend) used at 1:50 concentration; anti-F4/80 (Biorad) used at 1:250. Secondary antibody used: Alexa Fluor anti-mouse 488, Alexa Fluor anti-mouse 594, Alexa Fluor anti-rabbit 488, Alexa Fluor anti-rabbit 594, Alexa anti-goat 594 were all used at dilution 1:400 (ThermoFisher). Biotin goat anti-mouse IgG (Affinipure Jackson) was used at 1:1000 dilution; Cy3 strepdavidin was used at dilution 1:2500 (Affinipure Jackson).

Proteins extraction and Western blotting

Protein extracts from cells and from muscle (*quadriceps, diaphragms*) were lisated in extraction buffer (50 mM Tris HCl, 0,15 M NaCl, 5mM EDTA, 1% TritonX-100 in distilled water) plus protease inhibitors cocktail, Roche, and PMSF, Sigma). Muscles are homogenized with Tissueruptor (Quiagen). Extracts are then sonicated with a sonicator (100% amplitude , 30 ON/30 OFF for 10 cycles). Samples are then quantified for protein content according to BCA (Thermo Scientific). An aliquot of each sample was later treated with DNAseI (Thermo Scientific) to extract histons. The samples are incubated with DNAseI solution for 30 minutes at 37°C. All samples were later diluted with the loading samples buffer and are denatured for 5 minutes at 99 °C. The cell lysates were resolved on 4%–15% TGX gradient gels (Bio-Rad Laboratories) and transferred to nitrocellulose membrane (Amersham). Membranes were blocked with 5% non-fat dried milk in TBS with 0.2% Tween for 1 h at room temperature.Then the filter is incubated with the primary antibody overnight at 4 ° C, diluted in blocking solution. After washing in TBS with 0.2% Tween, membrane were incubated with specific HRP-conjugated secondary antibodies (Sigma) for 1h at RT. After washing in TBS with 0.2% Tween, blots were developed with Western lightning enhanced chemiluminescence (Thermo Fisher Scientific) and signal detected with ChemiDoc (BioRad). Primary antibodies used: H3K9me2 (Abcam) used 1:500; H3k9 Total (Abcam) 1:1000; Collagen3A1 (Santa Cruz) 1:500; MyHC (Mf20, DSHB) 1:20; GAPDH (Sigma), 1:5000.

FACS sorting and cell culture

The sorting of the two population used in this project, FAPs e MuSCs, is made in collaboration with Giovanna Peruzzi at Italian Institute of Technology (IIT). Cells were sorted using a

FACSAriaIII (Becton Dickinson, BD Biosciences) equipped with 488nm, 561nm and 633nm laser and FACSDiva software (BD Biosciences version 6.1.3). Data were analyzed using a FlowJo software (Tree Star, version 9.3.2).
As described in Fig.1B, to isolate primary cells, hindlimb muscles were homogenized (*Tibialis Anterior, Gastrocnemius, Quadriceps*) and digested in HBSS (Gibco) with 2 ug / ml Collagenase A (Roche) , 2.4 U / mL Dispase II (Roche) , 10 ug / mL DNase I (Roche) , 0.4 mM CaCl2 and 5mM MgCl2 for 1 h at 37 ° C in agitation. Samples are then resuspended in washing buffer HBBS with 0,2 % BSA / 1% penicillin-streptomycin (Sigma). Muscle slurries were passed 10 times through a 20G syringe (BD Bioscience). Cell suspension was obtained after three successive cell strainer filtrations with washing buffer. The pellets were resuspended in HBBS with 1 % DNAse and incubated over night at 4°C. Single cell suspension was stained the day after with CD45/CD31/Ter119 PE for lineage exclusion, Sca1-FITC and α7integrin APC Vio770, according to the experimental panel design. Satellite cells (MuSCs) were isolated as cell Ter119-/CD45-/CD31-/α7Integrin + / SCA1- ; the FAPs as Ter119-/CD45-/CD31-/α7Integrin-/Sca1+. Antibodies were used at the following concentrations: anti mouse CD31 (PECAM-1) PE, anti mouse CD45 - PE, Ter119 - PE (Miltenyi Biotec) all used at 1:25; anti mouse SCA-1 (Ly-6A) FITC(Miltenyi Biotec) 1:25 and α7Integrin – APC VIO770 (Miltenyi Biotec) 1:20.
Freshly sorted cells were plated on 1 mg/ml ECM Gel-coated dishes in Cyto-grow (Resnova) complete medium as a growth medium (GM). Satellites cells were shifted in differentiation medium with dmem pyr+ with 5% Horse Serum. For adipogenic differentiation (DM) of FAPs, generally after 7 days of GM, cells were exposed for 3 days to adipogenic induction medium (DMEM, 10% FBS, 0.5 mM IBMX, 0.25 mM dexamethasone and 10 mg/ml insulin), followed by further 3 days in adipogenic maintenance medium (DMEM, 10% FBS and 10 mg/ml insulin). For in vitro treatment, cells were treated for 48h with 1nM A-366 and 50nM M-108 in GM and then switched in DM without the drug. C2C12 cells were cultured in growth medium (DMEM 10%FBS), and in differentiation medium with DMEM, %2 horse serum.

Quantification and statistical analysis

All images were taken with optical microscope Nikon Eclipse TE300 and ZEISS Axio Observer 3/ Colibri7.The diameter of myotubes was evaluated by taking 3 measures along each myotube using ImageJ “straight” command, and then the average among the 3 measures was used as diameter of each myotube.
The Perilipin positive droplets, as well as Oil Red O area, were quantified using ImageJ, calculating the area of the red pixels ($pixel^2$) per field. The same procedure has been applied to evaluate the content of Collagen3A and Sirius Red positive areas. CSA is calculated using an ImageJ software plug-in (NIH) ImageJ + macro (Macro_seg_5_modif.ijm.txt). Areas are measured using images of sections taken randomly to cover the entire transverse area of the muscle; it is necessary to convert the values obtained in pixels into micron, thus obtaining the area of myofibers (um^2) per field. The same procedure, using the macro, was used to calculate the minimum Feret’s diameter of myofibers. The minimal “Feret’s diameter” is defined as closest possible distance between the two parallel tangents of an object (i.e. muscle fiber).
To quantify the content of MPO positive nuclei was used the count-nuclei plug-in of ImageJ software. To verify the presence of necrotic fibers, positive fibers for IgG were quantified with the multi-point tool of ImageJ software. The point-tool was also used to quantify the number of F4/80, CD206 and Pdgfr-alpha positive cells for field.

For western blot analysis quantification, images from Chemidoc (Biorad) are analized by ImageLab 6.0 software (Biorad), using the quantification tool, to obtain densitometry for lanes and bands. Quantification of protein expression levels was performed using GAPDH or H3 total protein level as a reference.

The statistical details of experiments can be found in the corresponding figure legends. All data are represented as mean ± standard error of the mean (s.e.m.). Graphs were created with Graphpad Prism 8, which was used for all statistical tests. The number of replicates (n) and the statistical test applied for each experiment is indicated in the figure legends. The differences were considered statistically significant when $P \leq 0.05$ and reported as follows: ****$P \leq 0.0001$, ***$P \leq 0.001$, **$P \leq 0.01$, *$P \leq 0.05$.

References

Aartsma-Rus A, van Putten M. ,(2014) Assessing functional performance in the mdx mouse model. J Vis Exp. (85).

Arrowsmith CH, Bountra C, Fish PV, Lee K, Schapira M (2012). Epigenetic protein families: a new frontier for drug discovery. Nat Rev Drug Discov. Apr 13;11(5):384-400.

Bettica P, Petrini S, D'Oria V, D'Amico A, Catteruccia M, Pane M, Sivo S, Magri F, Brajkovic S, Messina S, Vita GL, Gatti B, Moggio M, Puri PL, Rocchetti M, De Nicolao G, Vita G, Comi GP, Bertini E, Mercuri E (2016). Histological effects of givinostat in boys with Duchenne muscular dystrophy. Neuromuscul Disord. Oct;26(10):643-649.

Bresciani A, Ontoria JM, Biancofiore I, Cellucci A, Ciammaichella A, Di Marco A, Ferrigno F, Francone A, Malancona S, Monteagudo E, Nizi E, Pace P, Ponzi S, Rossetti I, Veneziano M, Summa V, Harper S. (2018). Improved Selective Class I HDAC and Novel Selective HDAC3 Inhibitors: Beyond Hydroxamic Acids and Benzamides. ACS Med Chem Lett. Nov 27;10(4):481-486.

Choi J, Jang H, Kim H, Lee JH, Kim ST, Cho EJ and Youn, HD (2014). Modulation of lysine methylation in myocyte enhancer factor 2 during skeletal muscle cell differentiation. Nucleic acids research *42*, 224-234.

Colussi C, Mozzetta C, Gurtner A, Illi B, Rosati J, Straino S, Ragone G, Pescatori M, Zaccagnini G, Antonini A, Minetti G, Martelli F, Piaggio G, Gallinari P, Steinkuhler C, Clementi E, Dell'Aversana C, Altucci L, Mai A, Capogrossi MC, Puri PL, Gaetano C. (2008) HDAC2 blockade by nitric oxide and histone deacetylase inhibitors reveals a common target in Duchenne muscular dystrophy treatment. *PNAS*, *105*, 19183–19187. doi:10.1073/pnas.0805514105

Consalvi S, Mozzetta C, Bettica P, Germani M, Fiorentini F, Del Bene F, Rocchetti M, Leoni F, Monzani V, Mascagni P, Puri PL, Saccone V (2013). Preclinical studies in the mdx mouse model of duchenne muscular dystrophy with the histone deacetylase inhibitor givinostat. Mol. Med. 20(19), 79–87.

Consalvi S, Saccone V, Mozzetta C (2014). Histone deacetylase inhibitors: a potential epigenetic treatment for Duchenne muscular dystrophy. Epigenomics-UK; 6: 547-60

De Bruin M, Smeulders MJ, Kreulen M, Huijing PA, Jaspers RT (2014). Intramuscular connective tissue differences in spastic and control muscle: a mechanical and histological study. PLoS ONE 9(6): e101038.

De Luca A (2012). Preclinical drug tests in the mdx mouse as a model of dystrophinopathies: an overview, Acta Myologica XXXI, 40-47

De Luca A, (2018). Use of treadmill and wheel exercise for impact on *mdx* mice phenotype SOP treatNMD, DMD_M.2.1.001. on treat-nmd.org.

Delcuve GP, Khan DH and Davie JR (2012) Roles of histone deacetylases in epigenetic regulation: emerging paradigms from studies with inhibitors. Clinical Epigenetics 4:5

Denti MA, Rosa A, D'Antona G, Sthandier O, De Angelis FG, Nicoletti C, Allocca M, Pansarasa O, Parente V, Musarò A, Auricchio A, Bottinelli R, Bozzoni I. (2006). Body-wide gene therapy of Duchenne muscular dystrophy in the *mdx* mouse model. Proc. Natl. Acad. Sci. USA. 103:3758-3763.

Gawlik KI (2018). At the crossroads of clinical and preclinical research for muscular dystrophy—are we closer to effective treatment for patients? Int J Mol Sci. 19(5):1490.

Grange RW, (2008). Use of treadmill and wheel exercise to assess dystrophic state. SOP treatNMD, DMD_M.2.1.003. on treat-nmd.org.

Grounds MD, Radley HG, Lynch GS, Nagaraju K, and De Luca A (2008). Towards developing standard operating procedures for pre-clinical testing in the mdx mouse model of Duchenne muscular dystrophy. Neurobiol Dis. 31:1–19.

Guiraud S, Davies KE (2017). Pharmacological advances for treatment in Duchenne muscular dystrophy. Curr Opin Pharmacol. Jun; 34:36-48.

Heredia JE, Mukundan L, Chen FM, Mueller AA, Deo RC, Locksley RM, Rando TA, and Chawla A (2013). Type 2 innate signals stimulate fibro/adipogenic progenitors to facilitate muscle regeneration. Cell *153*, 376-388.

Iezzi S, Di Padova M, Serra C, Caretti G, Simone C, Maklan E, Minetti G, Zhao P, Hoffman EP, Puri PL, Sartorelli V (2004). Deacetylase inhibitors increase muscle cell size by promoting myoblast recruitment and fusion through induction of follistatin. Dev Cell. May;6(5):673-84.

Joe AW, Yi L, Natarajan A, Le Grand F, So L, Wang J, Rudnicki MA, and Rossi FM (2010). Muscle injury activates resident fibro/adipogenic progenitors that facilitate myogenesis. Nat Cell Biol *12*, 153-163.

Kopinke D, Roberson EC, and Reiter JF (2017). Ciliary Hedgehog Signaling Restricts Injury-Induced Adipogenesis. Cell 170, 340-351 e312.

Ling BM, Bharathy N, Chung TK, Kok WK, Li S, Tan YH, Rao VK, Gopinadhan S, Sartorelli V, Walsh, MJ, et al. (2012a). Lysine methyltransferase G9a methylates the transcription factor MyoD and regulates skeletal muscle differentiation. Proc Natl Acad Sci U S A 109, 841-846.

Ling BM, Gopinadhan S, Kok WK, Shankar SR, Gopal P, Bharathy N, Wang Y, and Taneja R (2012b). G9a mediates Sharp-1-dependent inhibition of skeletal muscle differentiation. Mol Biol Cell *23*, 4778-4785.

Mercuri E, and Muntoni F (2013). Muscular dystrophies. Lancet *381*, 845-860

Minetti GC, Colussi C, Adami R, Serra C, Mozzetta C, Parente V, Fortuni S, Straino S, Sampaolesi M, Di Padova M, Illi B, Gallinari P, Steinkühler C, Capogrossi MC, Sartorelli V, Bottinelli R, Gaetano C, Puri PL. (2006). Functional and morphological recovery of dystrophic muscles in mice treated with deacetylase inhibitors. Nat. Med. 12:1147-1150.

Mozzetta C, Boyarchuk E, Pontis J, Ait-Si-Ali S (2015) Sound of silence: the properties and functions of repressive Lys methyltransferases. Nat Rev Mol Cell Bio Aug; 16: 499-513

Mozzetta C, Consalvi S, Saccone V, Tierney M, Diamantini A, Mitchell KJ, Marazzi G, Borsellino G, Battistini L, Sassoon D, et al. (2013). Fibroadipogenic progenitors mediate the ability of HDAC inhibitors to promote regeneration in dystrophic muscles of young, but not old Mdx mice. EMBO Mol. Med. 5(4), 626–639.

Mozzetta C, Minetti G, Puri PL (2009). Regenerative pharmacology in the treatment of genetic diseases: the paradigm of muscular dystrophy. Int J Biochem Cell Biol 41, 701-710.

Ohno H, Shinoda K, Ohyama K, Sharp LZ and Kajimura S (2013). EHMT1 controls brown adipose cell fate and thermogenesis through the PRDM16 complex. Nature 504, 163-167.

Pappano WN, Guo J, He Y, Ferguson D, Jagadeeswaran S, Osterling DJ, Gao W, Spence JK, Pliushchev M, Sweis RF, Buchanan FG, Michaelides MR, Shoemaker AR, Tse C, Chiang GG (2015). The Histone Methyltransferase Inhibitor A- 366 Uncovers a Role for G9a/GLP in the Epigenetics of Leukemia. PLoS One. 2015 Jul 6;10(7) :e0131716.

Saccone V, Consalvi S, Giordani L, Mozzetta C, Barozzi I, Sandoná M, Ryan T, Rojas-Muñoz A, Madaro L, Fasanaro P, Borsellino G, De Bardi M, Frigè G, Termanini A, Sun X, Rossant J, Bruneau BG, Mercola M, Minucci S, Puri PL. (2014) HDAC-regulated myomiRs control BAF60 variant exchange and direct the functional phenotype of fibro-adipogenic progenitors in dystrophic muscles. Genes Dev. Apr 15;28(8):841-57. doi: 10.1101/gad.234468.113.

Sartorelli V and Juan AH (2011). Sculpting chromatin beyond the double helix: epigenetic control of skeletal myogenesis. Curr Top Dev Biol. 2011;96:57-83. doi: 10.1016/B978-0-12-385940-2.00003-6.

Sartorelli V, Puri PL. (2018) Shaping Gene Expression by Landscaping Chromatin Architecture: Lessons from a Master. Mol Cell. 2018 Aug 2;71(3):375-388.

Shinkai Y, and Tachibana M (2011). H3K9 methyltransferase G9a and the related molecule GLP. Genes Dev 25, 781-788.

Sweis RF, Pliushchev M, Brown PJ, Guo J, Li F, Maag D, Petros AM, Soni NB, Tse C, Vedadi M, et al. (2014) Discovery and Development of Potent and Selective Inhibitors of Histone Methyltransferase G9a. ACS Med Chem Lett. 5(2):205–9.

Tachibana M, Ueda J, Fukuda M, Takeda N, Ohta T, Iwanari H, Sakihama T, Kodama T, Hamakubo T, and Shinkai Y (2005). Histone methyltransferases G9a and GLP form heteromeric complexes and are both crucial for methylation of euchromatin at H3-K9. Genes Dev 19, 815- 826.

Tidball JG, Welc SS, Wehling-Henricks M, (2018) Immunobiology of Inherited Muscular Dystrophies, Compr Physiol. 2018 Sep 14;8(4):1313-1356.

Tidball JG, (2017) Regulation of muscle growth and regeneration by the immune system, Nat Rev Immunol. March ; 17(3): 165–178.

Uezumi A, Fukada S, Yamamoto N, Takeda S, Tsuchida K. (2010) Mesenchymal progenitors distinct from satellite cells contribute to ectopic fat cell formation in skeletal muscle. Nat Cell Biol. Feb;12(2):143-52. doi: 10.1038/ncb2014.

Uezumi A, Ito T, Morikawa D, Shimizu N, Yoneda T, Segawa M, Yamaguchi M, Ogawa R, Matev MM, Miyagoe-Suzuki Y, et al. (2011). Fibrosis and adipogenesis originate from a common mesenchymal progenitor in skeletal muscle. J Cell Sci 124, 3654-3664.

Van Putten M, (2011). The use of hanging wire tests to monitor muscle strength and condition over time. SOP treaNMD, DMD_M.2.1.004. on treat-nmd.org.

Xu L, Park KH, Zhao L, Xu J, El Refaey M, Gao Y, Zhu H, Ma J, Han R. (2016). CRISPR-mediated Genome Editing Restores Dystrophin Expression and Function in mdx Mice. Mol Ther. Mar;24(3):564-9.

Glossary

DMD: Duchenne Muscular Dystrophy
KMT: Histone Lysine Methyltransferase
KMTi: Histone Lysine Methyltransferase inhibitor
HDAC: Histone deacetylase
HDACi: Histone deacetylase inhibitor
H3K9: Histone 3 Lysine 9
H3K9me2: Histone 3 Lysine 9 dimethylation
CTX: cardiotoxin
CSA: cross sectional area
MuSCs: Muscle Stem cells
FAPS: fibroadipogenic progenitors
IF: Immunofluorescence
TA: tibialis anterior
CK: creatinine kinase

SYNOPSIS

Epigenetic drugs as a pharmacological approach in Duchenne Muscular Dystrophy

Duchenne Muscular Dystrophy (DMD) is the most severe form of dystrophy that leads to progressive muscle weakness because of a gradual replacement of functional muscle with fat and fibrotic scars.

This pathology is caused by the absence of a functional Dystrophin in the sarcolemma, which therefore involves the inability of cells to sustain the mechanical stress of contraction resulting in muscle tissue degeneration (Mercuri and Muntoni, 2013). In a pathological condition such as DMD, dystrophin-deficient myofibres possess increased vulnerability to muscle contraction with consequent continuous cycle of degeneration and regeneration. At the first stage of the disease a compensatory MuSCs-mediated regenerative response counteracts the degeneration with formation of newly myofibers. However, as disease progresses muscle mass is replaced with fibrous and fat tissues and recent studies identified FAPs as the source of fibrotic and fatty infiltrates that accumulate in degenerating dystrophic muscles (Kopinke et al., 2017; Uezumi et al., 2011). Currently, there is no definitive cure for DMD and the current treatment is the administration of corticosteroids. Pharmacological therapies for DMD should therefore aim to counteract this fibro-adipogenic degeneration and to promote the compensatory regeneration to slow down progression of pathology. Although this kind of approach is not curative, one positive aspect is that pharmacological therapies targeting events downstream the genetic defects are potentially available for all patients without restrictions due to specificity in DMD mutations.

Previous works proved pre-clinical efficacy of pan-histone deacetylase inhibitors (HDACi) in the treatment of murine models of DMD, showing the ability of HDACi to counter disease progression and induce functional and morphological recovery. These studies paved the way for ongoing clinical trials on dystrophic boys but the use of pan-HDACi raises several concerns because of their lack of selectivity and the potential to induce adverse effects over longer period of treatment. Thus, an urgency in the field of epigenetic pharmacology is to develop more selective strategies. The observation that inhibition of class I HDACs is sufficient to exert most of the beneficial effects triggered by pan-HDACi (Colussi et al., 2008), suggests that improving selectivity of epigenetic therapy does not compromise efficacy but also could increase its effect.

In this scenario, more selective epigenetic targets are represented by the highly specific lysine methyl transferases (KMTs) (Mozzetta et al.2015). In particular, H3K9 KMTs are emerging as particularly relevant in myogenesis, among them the mono- and di-methyltransferase G9a and GLP (G9a-like protein) that act as a hetero-dimer (Shinkai and Tachibana, 2011; Tachibana et al.2005) are emerging as important modulators of gene expression during the differentiation of stem cells, thus imposing themselves as potential pharmacological targets for regenerative medicine. In the context of muscle differentiation, G9a and GLP have recently been identified among epigenetic modulators able to maintain the repression of muscle-specific genes both in embryonic precursors and in myoblasts (Ling et al., 2012a; Ling et al., 2012b; Ohno et al., 2013), thus preventing their premature differentiation and acting as spatio-temporal modulators of the myogenic differentiation program.

Therefore, the development of KMTs specific inhibitors might be a strategy to increase selectivity of epigenetic therapies. We aimed here to test pre-clinical efficacy of newly developed specific inhibitors for class I HDACs (I-HDACi) and H3K9 KMTs G9a/GLP (KMTi)

in murine models of skeletal muscle regeneration and DMD. We reasoned that modulation of these epigenetic modifiers could represent a way to promote the expression of muscle-specific genes and enhance muscle differentiation in cells or tissues whose myogenic capacity is compromised, such as DMD.

In agreement with our hypothesis, our data provide evidence of a pro-regenerative effect of these specific inhibitors *in vivo*. In particular, we show that compounds specific for G9a/GLP are able to enhance myogenesis *in vitro*. Moreover, we demonstrate that their delivery in vivo on murine models of acute muscle injury and DMD promote muscle regeneration and block accumulation of fibrotic, fatty and inflammatory infiltration. Moreover, dystrophic mice treated with KMTis displayed a reduced level of necrotic fibers and serum CK levels, suggesting a protecting effect of these compounds against muscle wasting. Importantly, KMTis induced beneficial effects also when administered at advanced stages of the disease, in old dystrophic mice. This evidence underscores the potential of these newly develop drugs in the treatment of DMD at advanced stages, when instead other pan epigenetic inhibitors are no longer effective.

Moreover, our data demonstrate pre-clinical efficacy of a newly designed specific inhibitor for class I HDACs. Our results show the capacity of this compound to promote the formation of bigger myofibers, to prevent fibro-adipogenic degeneration and inflammation, by inducing macrophages polarization towards an anti-inflammatory phenotype.

Taken together, our data suggest that the pharmacological treatment with more selective epigenetic drugs might become an effective therapeutic approach to counteract the degeneration in DMD. The results obtain with these novel epigenetic drugs suggest that these enzymes could represent a way to unlock the expression of muscle-specific genes and enhance muscle differentiation in pathological condition, such as DMD. Finally, the results gained by these studies will provide important insights to further develop these drugs and even to conceive future combined therapies targeting both HDACs and KMTs.